https://ntrs.nasa.gov/search.jsp?R=19660026369 2020-03-16T20:37:39+00:00Z

TECH LIBRARY KAFB, NM
0099369

NASA CONTRACTOR REPORT

NASA-GR-5
C.1

TECH LIBRARY KAFB, NM
AFWL (WLIL-2)
KIRTLAND AFB, N MEX

NASA CR-596

ESTIMATES OF NONEQUILIBRIUM IONIZATION PHENOMENA IN THE INVISCID APOLLO PLASMA SHEATH

by M. G. Dunn, J. W. Daiber, J. A. Lordi, and R. E. Mates

Prepared by
CORNELL AERONAUTICAL LABORATORY, INC.
Buffalo, N. Y.
for Goddard Space Flight Center

NATIONAL AERONAUTICS AND SPACE ADMINISTRATION • WASHINGTON, D. C. • SEPTEMBER 1966

TECH LIBRARY KAFB, NM
0099369

NASA CR-596

ESTIMATES OF NONEQUILIBRIUM IONIZATION PHENOMENA IN THE INVISCID APOLLO PLASMA SHEATH

By M. G. Dunn, J. W. Daiber, J. A. Lordi, and R. E. Mates

Distribution of this report is provided in the interest of information exchange. Responsibility for the contents resides in the author or organization that prepared it.

Prepared under Contract No. NAS 5-3976 by
CORNELL AERONAUTICAL LABORATORY, INC.
Buffalo, N.Y.

for Goddard Space Flight Center

NATIONAL AERONAUTICS AND SPACE ADMINISTRATION

For sale by the Clearinghouse for Federal Scientific and Technical Information
Springfield, Virginia 22151 – Price $2.50

TABLE OF CONTENTS

Section		Page
	FOREWORD	v
	ABSTRACT	vii
1.	INTRODUCTION	1
2.	METHOD OF CALCULATION	3
	2.1 Flow Field	3
	2.2 Streamtube Calculations	4
	2.3 Air Chemistry Model	7
3.	RESULTS	9
	3.1 Basic Chemical Kinetics	9
	3.2 Streamline Species Distributions for 2000,000 ft.	10
	3.3 Electromagnetic Propagation in Plasma Sheath	13
	3.4 Streamline Species Distributions for 250,000 ft.	15
	3.5 Determination of Important Chemical Reactions	17
4.	CONCLUDING REMARKS	21
	REFERENCES	23
	TABLES	25
	FIGURES	29

FOREWARD

The work described in this report was supported by the National Aeronautics and Space Administration, Goddard Space Flight Center, under Contract NAS 5-3976.

The material contained herein was presented at the Third Symposium on the Plasma Sheath - Plasma Electromagnetics and Hypersonic Flight, sponsored by the Air Force Cambridge Research Laboratories at Boston, Massachusetts, September 21-23, 1965.

The authors wish to acknowledge the assistance of J. R. Moselle in carrying out the numerical solutions discussed in this report.

ABSTRACT

Estimates of nonequilibrium ionization phenomena in the asymmetric plasma sheath have been made for an Apollo-type body entering the earth's atmosphere at superorbital velocity. For an entry velocity of 30,000 ft/sec and an attack angle of 20°, results are presented for altitudes of 200,000 ft and 250,000 ft. for the pitch plane.

The charged species are taken as N_2^+, O_2^+, NO^+, N^+, O^+ and e^-. The chemical model employed permits three-body recombination reactions, two-body dissociative-recombination reactions, charge-exchange reactions, and ion-atom-exchange reactions. Nonequilibrium species concentrations for both the neutral and the charged particles are presented along several streamlines for both altitudes investigated. The species distributions have a defined pattern which is readily interpreted in terms of the local temperature, velocity, and density fields. With the exception of the body stagnation point and a relatively small region on the body surface, the plasma-sheath fluid is found to be in a nonequilibrium state. The dominant electron-depletion reactions are shown to be $NO^+ + e^- \rightarrow N + O$, $N_2^+ + e^- \rightarrow N + N$, $N^+ + e^- + e^- \rightarrow N + e^-$, and $O^+ + e^- + e^- \rightarrow O + e^-$. Other important chemical reactions involving the charged species are discussed for various portions of the plasma sheath.

Contours of electron density in the forebody and near afterbody region are presented for altitudes of 200,000 ft. and 250,000 ft. For the 200,000 ft. case, the maximum forebody electron density in the stagnation region is calculated to be approximately 5×10^{15} electrons/cm^3. In the windward corner region the electron density is on the order of 5×10^{13} electrons/cm^3 and in the leeward corner region, is approximately 5×10^{12} electrons/cm^3. Corresponding values of electron density for an altitude of 250,000 ft. are found to be approximately 50 times less.

Electron-neutral and electron-ion collision frequencies are also calculated along each streamline in the plane of symmetry. The solution for an altitude of 200,000 ft. indicated a maximum electron-neurtral collision frequency in excess of 1×10^{10} rad/sec in the forebody region. In the corner region the electron-neutral collision frequencies are on the order of 5×10^{9} rad/sec. The electron-ion collision frequencies in the forebody region are slightly less than the electron-neutral collision frequencies for the same region. The corner region values are approximately one-fifth the corresponding electron-neutral collision frequencies. Similar calculations are conducted for an altitude of 250,000 ft. For a given streamline the electron-neutral collision frequencies are found to be approximately an order of magnitude less than at 200,000 ft. The electron-ion collision frequencies are found to be approximately 1/100 those for corresponding plasma sheath locations at 200,000 ft.

The electron density distribution and the collision frequency distribution for two selected paths through the plasma sheath are presented. The peak electron densities and collision frequencies for these paths occur at a significant distance from the body. The high electron density and collision frequencies in the inviscid flow-field emphasize the importance of the inviscid flow-field chemical kinetics. Additionally, they suggest that the influence of ablation products and viscous effects on the electromagnetic propagation should be more closely evaluated.

The attenuation for the propagation of one-dimensional plane waves along these two paths is presented. The implication of these results is that for the particular trajectory position and transmission paths selected it would be exceedingly difficult to communicate with the craft at a carrier frequency in the range of 1 to 10 Gc.

LIST OF SYMBOLS

A	Avogadro's number
A_i	constant term in reaction rate constant of i^{th} reaction
$\bar{c}$	mean electron speed
H	total enthalpy
h	static enthalpy
k	Boltzmann's constant
k_{F_i}	forward rate constant of i^{th} reaction
ℓ	characteristic length
M	collision partner
m_e	mass of an electron
n_e	local electron density
n_i	temperature exponent in reaction rate constant of i^{th} reaction
n_j	particle density of j^{th} species
P	streamline static pressure
P_o'	streamline static pressure immediately behind translational shock
P_i	defined by Eq. 10
Q_j	electron-neutral scattering cross-section for j^{th} species
Q_{ion}	electron-ion scattering cross-section (defined by Eq. 6)
R_{f_i}	forward rate of i^{th} reaction
R_{r_i}	reverse rate of i^{th} reaction
T	temperature
u_t	tangential velocity component
u_n	normal velocity component
x	distance along streamline

$\bar{x}$	non-dimensional distance along streamline, x/ℓ
β_{ij}	defined by Eq. 9
γ	species concentration
γ_j^+	concentration of j^{th} charged species
θ_i	activation energy of i^{th} reaction
ν_{ij}	stoichiometric coefficient of the j^{th} species on the reactant side of the i^{th} reaction
ν'_{ij}	stoichiometric coefficient of the j^{th} species on the product side of the i^{th} reaction
ν	electron-neutral collision frequency (defined by Eq. 5)
ν^+	electron-ion collision frequency (defined by Eq. 7)
ρ	density
τ_i	defined by Eq. 11

Subscripts

∞	evaluated at free-stream conditions
2	evaluated downstream of translational shock

1. INTRODUCTION

Previous experience with the Mercury and Gemini earth-orbiting space vehicles which entered the atmosphere at a maximum velocity of approximately 24,000 ft/sec has indicated that communication with the craft at customary radio frequencies is impossible during a significant portion of the entry trajectory due to free electrons in the plasma sheath. Future entry conditions such as the 36,000 ft/sec superorbital velocity typical of the Apollo return from lunar missions imply considerable higher plasma-sheath electron densities than previously experienced. Thus, the blackout period of radio-frequency transmission can be expected to increase. If accurate estimates of the blackout boundaries are to be made, it is necessary that the ionization kinetics occurring within the plasma sheath be understood.

The purpose of this paper is to present detailed estimates of nonequilibrium ionization phenomena which have been obtained as part of an extensive study being conducted at CAL to investigate the asymmetric flow-field associated with an Apollo-type body at angle of attack. The objective of these estimates was to aid in the formulation of meaningful experiments and theoretical models of the plasma-sheath. With regards to the experiments, the important plasma-sheath electron production and depletion reactions are to be determined. For the theoretical models, it is necessary to obtain preliminary estimates of the flow field chemical composition and to determine those chemical reactions that must be included in future more exact calculations. A further goal is to obtain estimates of electron density and collision frequency distributions in the plasma sheath to aid in theoretical and experimental studies of electromagnetic propagation in dense plasmas.

In the present study, nonequilibrium ionization phenomena were calculated along fourteen streamlines in the pitch plane of an Apollo-type, asymmetric plasma sheath. The location of these streamlines in the plasma sheath and their corresponding pressure distributions were determined from an exact solution to the ideal-gas asymmetric flow field. This solution has been obtained using a time dependent direct method developed by Bohachevsky

and Mates[1,2] under support of the theoretical phase of this contract. The particular solution utilized was for a 30,000 ft/sec ideal-gas flow over an Apollo-type body at 20° angle of attack. The effects of the viscous boundary layer and the injection of ablation products were not included. For the given streamline pressure distribution an exact nonequilibrium ionization calculation was carried out using a streamtube computer program previously developed at CAL.[3]

Nonequilibrium species concentrations are presented for several of these streamlines for altitudes of 200,000 ft. and 250,000 ft. Contours of plasma sheath electron density determined from these calculations are presented for both altitudes. Corresponding electron-neutral and electron-ion collision frequencies are presented for selected streamlines. The results are then used to obtain electron density and collision frequency distributions along two paths through the plasma sheath. These distributions are utilized to calculate the attenuation of one-dimensional plane waves along the two paths.

These results are new in that an exact flow field solution for a blunt body at angle of attack was available so that a more realistic calculation of the plasma sheath ionization could be made. In view of this better flow field solution, a relatively complete air chemistry model was employed to perform the nonequilibrium ionization calculations along selected streamlines in the plane of symmetry.

2. METHOD OF CALCULATION

2.1 Flow Field

The time-dependent direct method[1,2] utilized to describe the asymmetric plasma sheath is founded on the principle that the physically correct steady-state solution is obtainable in the limit, for large time, of an appropriate nonsteady or transient solution. The technique starts the body from rest at time zero with constant velocity. The resulting nonsteady field is then computed until the desired steady-state solution is attained (i.e., when the flow field ceases to change). The retention of the time derivatives in the governing conservation equations results in a system of hyperbolic differential equations. Therefore, arbitrary free-stream parameters can be specified everywhere, except at the body, where the normal component of the velocity must vanish. This method describes the inviscid flow field for an arbitrary body shape with an arbitrary orientation.

The time-dependent direct method has been used to calculate the ideal-gas flow field for an Apollo-type vehicle at 20° angle of attack and a free-stream velocity of 30,000 ft/sec at an altitude of 200,000 ft. Bohachevsky and Mates[2] have located streamlines in the plane of symmetry and on the body surface. Figure 1, taken from their work, is presented here to illustrate the sonic line locations and the relative position in the plasma sheath of the fourteen streamlines used in the present study. The corresponding pressure distributions for these streamlines have also been determined and were used to calculate the plasma-sheath, nonequilibrium chemical kinetics by means of a streamtube technique. The details of this calculation are described in the next section.

In order to perform the nonequilibrium ionization calculation at 250,000 ft. it was assumed that the shock shape, shock standoff distance, and location of streamlines within the plasma sheath were identical to those in the 200,000 ft. solution. It was further assumed that the respective streamline pressure ratios P_2/P_o', where P_o' is the pressure immediately behind the shock for a given streamline, remained unchanged. However, the values of P_o' were evaluated for each streamline at both altitudes.

Of course, the present calculations do not include the effects of real gas phenomena on the basic gas dynamic characteristics of the flow field, such as shock shape and streamline geometry. However, it is felt that inclusion of such effects would not significantly alter the basic nature of the results.

2.2 Streamtube Calculations

The gasdynamic properties and flow composition along selected streamlines in the plasma sheath were obtained in the following manner. The previously described pressure distributions were used as input data to the CAL computer program which has been developed for numerical solutions of the quasi-one-dimensional, inviscid flow of reacting mixtures.[3,4] This program computes the flow of a general mixture of ideal gases through a streamtube of specified cross section or one having a specified streamwise pressure variation. The vibrational and electronic degrees of freedom are assumed to remain in thermal equilibrium with translation while the chemical reactions proceed at finite rates. Ionized mixtures are treated by considering electrons to be a separate chemical element.

In performing the nonequilibrium ionization calculations it was necessary to assume that the free-electron temperature was equal to the gas translational, vibrational, and electronic temperature. There is reason to believe that this assumption may not be valid on the basis of Daiber's studies[5] of the dissociative recombination of NO^+ in an expanding nozzle flow using microwave techniques. The results of that work indicated that the electron temperature is most likely higher than the gas translational temperature. Hurle and Russo[6] studied the coupling between free-electron temperature and N_2 vibrational temperature in expanding flows using a spectrum-line reversal technique. They concluded that in the presence of trace amounts of N_2 the electron temperature and the nitrogen vibrational temperature were essentially equal but higher than the translational temperature. At this time it is not possible to estimate the influence of this uncertainty on the electron density distributions. Additional research is underway at CAL to determine the effect of such energy coupling on the chemical kinetics.

In the streamtube computer program the enthalpy and chemical potential of each species are specified. In addition to the reaction-rate information, it is necessary to specify data for the thermodynamic properties of the species. Since the gas is assumed to be a mixture of ideal gases, the species properties must be specified functions of temperature only. Two methods are used to describe the species thermodynamic properties: polynomial fits to tabulated data or alternately, a simple harmonic-oscillator model. In the present calculation the polynomial fits to tabulated data were used for temperatures between 6000°K and 24,000°K and the harmonic-oscillator model was used below 6000°K. The polynomial fits employed were those obtained by Marrone[7] from the tabulated data of Gilmore.[8] The species data used in the harmonic-oscillator model are given by Marrone.[9]

In addition to the specification of the streamline pressure distribution and the chemical model, the streamtube computer program requires the specification of initial conditions. For the present study, the initial point of the calculation is just behind the translational, rotational shock. The vibrational and electronic degrees of freedom were assumed to attain equilibrium with the translational and rotational mode prior to any chemical reaction.

The pressure at the initial post-shock position was taken to be the value immediately behind the shock in the ideal-gas solution. Then, using this pressure P_o' and the free-stream conditions, the velocity components u_{t2} and u_{n2} were evaluated from the oblique shock relations.

$$u_{t2} = u_{t\infty} \tag{1}$$

$$u_{n2} = u_{n\infty} - \frac{P_2 - P_\infty}{\rho_\infty u_{n\infty}} \qquad \text{(for this condition } P_2 = P_o'\text{)} \tag{2}$$

The velocity components ahead of the shock are given by $u_{t\infty} = u_{\infty} \cos \theta$ and $u_{n\infty} = u_{\infty} \sin \theta$ where θ is the angle the tangent to the shock makes with the free-stream velocity vector. Then the static enthapy behind the shock is obtained from

$$h_2 + \frac{u_2^2}{2} = (H_o)_{\infty} \tag{3}$$

where $u_2^2 = u_{n2}^2 + u_{t2}^2$ and $(H_o)_{\infty}$ is the total enthalpy of the freestream.

In order to find the temperature consistent with the condition of vibrational and electronic equilibrium at the initial point, the following procedure was adopted. Using the polynomial fits to the thermodynamic data of N_2, O_2, and Ar the quantity

$$h(T) = (\gamma_{O_2})_{\infty} h_{O_2}(T) + (\gamma_{N_2})_{\infty} h_{N_2}(T) + (\gamma_{Ar})_{\infty} h_{Ar}(T) \tag{4}$$

was plotted as a function of temperature. The variables $(\gamma_{O_2})_{\infty}$, $(\gamma_{N_2})_{\infty}$ and $(\gamma_{Ar})_{\infty}$ represent the free-stream concentrations in moles/gm and h_{O_2}, h_{N_2}, h_{Ar} represent the species enthalpies in cal/mole. Then T_2 was obtained from the calculated value of h_2 using this graph of h versus T. Using P_o', T_2, and assuming the composition to be frozen at the free-stream values, the density at the initial point, ρ_2, was calculated from the state equation.

Typical streamline pressure distributions are illustrated in Figures 2, 3, and 4. The relative location of these streamlines in the plasma sheath is illustrated by the insert. The pressure distribution has been nondimensionalized by dividing the local static pressure, P_2, by P_o'. Polynominal fits to the streamline pressure distributions were obtained and used as input data to the streamtube program. Any discrepancies between the polynomial fits and the ideal-gas solution were comparable to the approximation that the nonequilibrium effect on the pressure distribution was negligible.

2.3 Air Chemistry Model

Table I presents the chemical kinetic data utilized for reactions involving neutral species. The rate constants used in these calculations were taken from Eschenroeder, Boyer, and Hall[3] and by Hall, Eschenroeder and Marrone.[10] The neutral species permitted in this model are N_2, O_2, NO, N, O, and Ar. It will be illustrated later that the species concentrations of the neutral particles N and O are, in general, an order of magnitude or two greater than the electron concentration. Thus, the neutral chemistry has a significant influence on the streamline gas dynamics and hence on the ionization kinetics.

Table II defines the chemical kinetic data utilized for reactions involving charged species. The charged species are taken to be N_2^+, O_2^+, NO^+, O^+ and e^-. The model employed permits three-body recombination reactions, two-body dissociative-recombination reactions, charge-exchange reactions, and ion-atom exchange reactions. The rate constants presented in Table II were taken from the published literature.[11-14]

Rate constants for the dissociation of N_2 and O_2 and the formation of NO are generally considered to be better known than those for chemical reactions involving charged particles. These reactions involving only neutral species have been measured for relatively high gas temperatures. The recombination rates, however, for these species have not been measured for high-temperature expanding flows. It is difficult to determine the rate-constant uncertainty for reactions involving neutral species but it is estimated to be less than an order of magnitude.

The uncertainty in the ionized-species reaction-rate constants is significantly greater than that of the neutral chemistry model. Table III presents a comparison at selected temperatures for six of the charged species chemical reactions which were found to be important in the plasma sheath. Many other reactions were found to be important but not as consistently so as those included in this comparison. The results of this comparison indicate that the rate constant value can differ by several orders of magnitude depending on the source one selects.

The influence of rate-constant uncertainty on the streamtube electron-density distribution for an expanding flow, using the complete chemical model given in Tables I and II, has been investigated as part of the present program at CAL. The rate constants for the charge-exchange reactions and the three-body, electron-ion recombination reactions were independently perturbed by two orders of magnitude. The results of these calculations indicated that such an uncertainty can have an order of magnitude influence on the streamtube electron distribution. Bortner[15] has previously determined that an order of magnitude variation in the O_2 dissociation rate constant can change the electron density by two orders of magnitude. He further illustrates that an order of magnitude decrease in the NO^+ ionization reaction rate (NO^+ is the only ion considered in his model) results in a corresponding order of magnitude decrease in the electron density. It has thus been illustrated that the rate constant uncertainty has a significant influence on the plasma sheath electron density. From a communication viewpoint this uncertainty is quite important. This is the reason for the experimental program currently underway at CAL to measure the important chemical reaction rate constants for Apollo-type plasmas.

The largest rate-constant uncertainty illustrated by Table III is that for the three-body, electron-electron-ion recombination reactions. This particular reaction was found to be important near the body corner in the region of rapid expansion. However, the reverse of this reaction was found to be a dominant source of electrons in the forebody region. Several authors[13, 16] have published predictions of the rate constant for the electron recombination reaction. In addition, Hinnov and Herschberg[17] have studied the three-body recombination rate of He^+ in the quiescent afterglow of the B-1 stellarator discharge. In light of current information on this particular reaction, it makes little difference whether the ion is He^+, H^+, O^+, or N^+. The rate constants proposed by Makin and Keck,[13] Bates, Kingston, and McWhirter,[16] and Hinnov and Herschberg[17] are all in agreement. Bortner[14] also suggests a value for the electron-electron-ion recombination rate constant. However, in view of the results of References 13, 16 and 17 the value suggested by Makin and Keck[13] has been utilized in this study.

3. RESULTS

3.1 Basic Chemical Kinetics

Before discussing in detail the nonequilibrium ionization results, a few remarks concerning general aspects of the streamtube chemistry are in order. In a gross sense, the nonequilibrium streamtube species distributions should be expected to illustrate trends similar to the more familiar normal shock solutions as modified by the gas dynamic environment of the curved shock layer. The gas passing through the more normal portion of the translational shock can be expected to experience significantly more molecular dissociation than the flow passing through the outer extremities as a result of the higher static temperature associated with the stagnation region. As dissociation proceeds in these streamtubes the static temperature decreases and the rate of dissociation also decreases. The higher temperature streamtubes should also have correspondingly higher ionized species concentrations as a result of their greater internal energy.

Streamtubes in the immediate vicinity of the stagnation region and in close proximity to the body surface are the most likely locations for the occurence of a local equilibrium state as a result of the higher temperature and increased residence time of the fluid. Obviously, at the inviscid stagnation point, where the velocity becomes zero, the fluid achieves equilibrium. The peak ionization along the inner streamtubes should occur at shorter streamtube distances from the shock than the corresponding peaks for the extremity streamtubes as a result of the lower fluid velocities and higher temperature. With regard to the influence of ambient density on the chemical kinetics it should be expected that if equilibrium is achieved the respective streamtube temperatures will be decreased. Molecular dissociation can be expected to become more complete and the charged species concentrations should increase. For a given streamtube, a reduction of the initial density effectively reduces the number of particle collisions and can be expected to increase the streamtube distance required to achieve maximum ionization.

3.2 Streamline Species Distributions for 200,000 ft.

This section discusses the calculated neutral and charged species distributions for 200,000 ft. altitude. Typical results for the neutral species are presented in Figs. 5, 6, and 7 for streamlines, 10, 3, and 14 (see Fig. 1 for relative location of streamlines). These results illustrate that for the higher static temperature streamlines (10 and 3) the dissociation of N_2 and O_2 is greater than it is for the lower temperature streamline 14. The maximum neutral species concentrations were found to be approximately an order of magnitude greater than the maximum charged-particle species concentrations. Thus, the neutral chemistry has a strong influence on the thermodynamic properties of the plasma and the ionization kinetics. Near the end of each of the streamlines the atomic species N and O and the N_2 molecule tend to a constant concentration. However, the molecular species NO and O_2 do not illustrate this trend.

Figures 8 and 9 illustrate the charged species distributions along streamlines 5 and 3 in the windward plasma sheath. Because of the relatively high temperature of streamline 5, the maximum electron concentration along this streamline is approximately four times greater than that along streamline 3. The peak concentration is attained in approximately one-fourth the corresponding distance for streamline 3 as a result of the lower streamtube velocity. The difference in the pressure distribution for these two streamlines is unimportant as regards to streamline chemistry.

Figure 8 illustrates that for the first centimeter along the streamline the dominant ion is N_2^+. After 5 centimeters the dominant ion becomes N^+. The initial concentration of O_2^+ is slightly greater than the NO^+ concentration. However, O_2^+ is depleted so rapidly that at a distance of 100 centimeters its concentration is several orders of magnitude less than the other ions.

The species distributions along streamline 3 are indicative of the lower temperature streamlines. The electron concentration at the shock is significantly lower than in the previous case. Again the dominant ion in the first centimeter is N_2^+. Further along the streamline NO^+, N^+, and

O^+ become the dominant ions. The species distribution presented in Figures and 9 do not give indications of a chemically frozen flow. In addition, the fluid along these streamlines is far from equilibrium as determined by evaluating the ratio of the forward to the reverse reaction rate for each reaction at selected points along the streamlines. The forward and reverse rates were in all cases significantly different.

Figures 10, 11, and 12 present species distributions along three streamlines in the leeward portion of the flow field. The distributions are presented in order of decreasing streamtube static temperature. Streamline 8 is the streamline that wets the leeward body surface. The maximum electron concentration for streamline 8 is 3.5 times greater than that for streamline 12 and 200 times greater than that for streamline 14. The peak electron concentration is observed to occur much closer to the shock for the higher temperature streamlines, once again illustrating the influence of temperature and local velocity on the chemical kinetics.

Figure 10 indicates that as the gas expands along the leeward forebody surface the electron concentration remains relatively constant until the corner region is reached. In the vicinity of the corner the gas begins to expand and rapid changes in species concentration are observed. The ratio of the forward to the reverse reaction rate was also investigated for the streamline. At a distance of approximately 100 centimeters from the translational shock a local equilibrium was approached. This is the only location within the entire flowfield, with the exception of the inviscid stagnation point, where local equilibrium was approached. The species distribution for streamline 12, which is shown in Figure 11, does not exhibit a pronounced region of constant electron concentration. However, the influence of the corner expansion on the species concentrations is observed in the rapid decrease of species concentration near the end of the streamline. Figure 12 illustrates that for streamline 14, the minimum static temperature line investigated, approximately 100 centimeters of streamline travel were required for the electron concentration to reach its maximum. The ionized species concentrations are decreasing rapidly at 250 centimeters, the terminal point of the calculation.

From Figures 10, 11, and 12, the dominant ion near the shock was determined to be N_2^+. Further along streamline 8 the dominant ions were found to be the atomic ions N^+ and O^+. At distances greater than 10 centimeters along streamline 12 the ions N^+, O^+, and NO^+ were of approximately the same order of magnitude. Figure 12 indicates that beyond 10 centimeters along streamline 14 the dominant ion is clearly NO^+.

The results presented above can be summarized by noting that several regions exist in which the dominant charged species are different. Immediately behind the translational shock a molecular ionization region was found for all streamlines. For the fluid passing through the more normal portion of the shock this molecular ionization region is followed by an atomic ionization region within a short distance behind the shock. For streamlines crossing the translational shock intermediate to the near-normal and outer portion, this molecular ionization region is followed by a combined molecular and atomic ionization zone in which N_2^+, N^+, NO^+, and O^+ become the dominant ions. In the case of the outer extremity streamlines the molecular ions N_2^+ and O_2^+ are significantly depleted and the dominant ion becomes NO^+ instead of the atomic ions N^+ and O^+. These regions are classified, the dominant ions noted, and the chemical reactions responsible for these trends discussed in detail in Section 3.5 and summarized in Table IV.

Contours of forebody electron density were constructed using the streamline species distributions and are presented in Figure 13 for an altitude of 200,000 ft. at a velocity of 30,000 ft/sec. In the stagnation region the electron density is in excess of 1×10^{15} electrons/cm^3 but less than 5×10^{15} electrons/cm^3. The windward-side electron density in the corner region varies from approximately 1×10^{15} to 5×10^{13} electrons/cm^3. The flow-field solution used for the nonequilibrium calculations has not, at this time, been extended to include more of the afterbody flow. Thus, the windward, contours for lower than 5×10^{13} are not available. Leeward side contours are presented for electron densities from 1×10^{15} to approximately 5×10^{12}

3.3 Electromagnetic Propagation in Plasma Sheath

In addition to calculating nonequilibrium species concentrations along each streamline, the electron-neutral and electron-ion collision frequencies were also calculated. The electron-neutral scattering cross sections Q_j used in this work were obtained by suitably averaging.[18, 19] the mono-energetic values suggested by Shkarofsky, et al[20]. The electron-neutral collision frequency as a function of position on a given streamline was then determined by the relation

$$\nu = \bar{c} \sum_j n_j Q_j \qquad \text{rad/sec} \qquad (5)$$

where the mean electron speed $\bar{c}$ is given by $\frac{4}{3}\sqrt{\frac{8kT_e}{\pi m_e}}$, the neutral particle density n_j is given by $\rho A \gamma_j$, A is Avogadro's number; and T_e is the electron temperature. The electron-ion scattering cross sections were calculated from Eq. (6) using the method suggested by Spitzer[21] and including the additional term suggested by Lin[22] to account for close collisions.

$$Q_{ion} = \frac{2.51}{T_e^2} \times 10^{-6} \ln\left[\frac{8.77 \times 10^3 (T_e)^{1.5}}{(n_j)^{0.5}}\right] + \frac{9.74 \times 10^{-7}}{T_e^2} \qquad (6)$$

The electron-ion collision frequency was then calculated as a function of position along the streamline using Eq. (7).

$$\nu^+ = \bar{c}\, n_e\, Q_{ion} \qquad \text{rad/sec} \qquad (7)$$

where $\bar{c}$ is given above and n_e is the local electron density in particles/cm^3.

In these calculations, as well as in the calculation of species concentration, the electron temperature T_e is assumed equal to the gas translational temperature.

Figures 14 and 15 present the electron-neutral and the electron-ion collision frequencies in the plane of symmetry for a free-stream velocity of 30,000 ft/sec at an altitude of 200,000 ft and an angle of attack of 20°. The electron-neutral collision frequency was somewhat in excess of 1×10^{10} rad/sec in the forebody region and in the corner region is on the order of 5×10^{9} rad/sec. The electron-ion collision frequency in the forebody region is slightly less than the electron-neutral collision frequency in the same region. However, the corner values are approximately a factor of five less than the electron-neutral collision frequencies.

The electron density distribution and the collision frequency (electron-neutral plus electron-ion) distribution for two selected paths through the plasma sheath have been calculated. Figure 13 illustrates the relative location of path "A" and path "B". Figures 16 and 17 present the electron density distribution and the collision frequency distribution for path "A". The peak electron density for path "A" is approximately 2×10^{14} electrons/cm^3 and occurs at approximately 60 centimeters from the body. As the shock is approached the electron density decreases rapidly. On the other hand, the collision frequency for path "A" is relatively constant through the plasma sheath. The peak value is approximately 1.1×10^{10} rad/sec at 60 centimeters from the body and the minimum value is 5×10^{9} rad/sec just behind the translational shock. Path "B" results are given in Figs. 18 and 19. The plasma is almost twice as thick as in the previous path. The maximum electron density for path "B" is 6×10^{13} and occurs at approximately 20 centimeters from the body. The maximum collision frequency for path "B" is also less than that for path "A". A maximum value of 6.5×10^{9} rad/sec occurs at 70 centimeters from the body.

The fact that the peak electron densities and collision frequencies for these paths occur at a significant distance from the body is important. The values of the peak electron densities and collision frequencies are high emphasizing the importance of the inviscid flow field. For the purposes of communication, the influence of ablation products and viscous effects on the electromagnetic-propagation should be compared to that of the inviscid flow field.

The attenuation for the propagation of one-dimensional plane waves along path "A" and path "B" has been calculated using a technique suggested by Bein[23]. Application of the technique requires that the electron density and collision frequency gradients normal to the direction of electromagnetic propagation be negligible. This condition was not met for the plasma sheath of interest in this work. Although realizing the limitations of its application to the plasma of interest, the technique was used to obtain qualitative estimates of the attenuation of plane electromagnetic waves. Calculations were initiated at a frequency of 9.0×10^{11} cycles/sec. The frequency was decreased until the attenuation exceeded approximately - 115 db. Calculations were also attempted at 3 Mc and 30 Mc. For these low frequencies the reflection coefficients approach unity. These could probably be reduced by properly matching the near field of the antenna to the plasma. However, the calculated absorption losses in the plasma were in excess of -150 db so that electromagnetic propagation at these frequencies still appears difficult.

Figure 20 presents the plasma sheath attenuation of the electromagnetic propagation as a function of carrier frequency for path "A" and path "B". These results indicate that the attenuation exceeds - 70 db for carrier frequencies less than 175 Gc along path "A" and 100 Gc along path "B". The implication of these results is that for this trajectory position and transmission path it would be exceedingly difficult to communicate with the craft at a carrier frequency in the range of 1 to 10 Gc. However, it must be emphasized that the accuracy of the electromagnetic-propagation calculation leading to the attenuation prediction is presently unknown. Before accurate estimates of the transmission and reflection coefficients can be made for plasmas of this type, a significant amount of theoretical and experimental research must be completed in the area of electromagnetic propagation.

3.4 Streamline Species Distributions for 250,000 ft.

Nonequilibrium ionization calculations for an altitude of 250,000 ft. were also performed. The shock shape, the relative position of the streamlines within the plasma sheath, and the nondimensional pressure distribution along the streamlines were assumed to be the same as for the 200,000 ft. case. Of course, the significant reduction of free-stream pressure, temperature, and density were accounted for in the calculations.

Nonequilibrium charged-species distributions along the windward streamlines 5 and 3 are presented in Figures 21 and 22. The electron concentration is increasing for almost the entire length of the streamlines. For a distance of approximately 10 centimeters along the streamlines the molecular ions N_2^+ and O_2^+ are dominant. At distances greater than 10 centimeters the molecular ions NO^+ and N_2^+ and the atomic ions N^+ and O^+ become dominant. The observed trend is similar to the 200,000 ft. results except that peak ionization for the higher altitude is achieved much further along the streamline. This is indicative of the lower density and thus fewer particle collisions. Figures 23 and 24 present the species distributions along the leeward streamlines 8 and 12. At relatively short distances along the streamlines the dominant ions are N_2^+, O_2^+, and NO^+. Near the end of the calculation the dominant ions are in general N^+, NO^+, N_2^+ and O^+. Thus once again the qualitative results are similar to the 200,000 ft. results except for the greater distance required to achieve peak ionization.

If the fluid flow were in equilibrium the streamline charged species concentrations for the 250,000 ft. calculations should have been greater than corresponding values at 200,000 ft. This, in fact, was not the case. Charged species concentrations for the 200,000 ft. case were in all cases greater than those for 250,000 ft. It is thus noted that the flow field at 250,000 ft. is also far from equilibrium. This conclusion was verified by reviewing the ratio of the forward and reverse reaction rates along the streamline.

The plasma-sheath electron density contours for 250,000 ft. altitude are presented in Figure 25. Both the maximum electron concentrations and the electron densities for a given streamline are less for this higher altitude case. The plasma-sheath electron densities for corresponding locations are 10 to 50 times less than for the 200,000 ft. case. Portions of the contours in the leeward region are dotted indicating an uncertainty in their location.

Electron-neutral and electron-ion collision frequencies for this higher altitude are presented in Figures 26 and 27 respectively. For a given streamline the electron-neutral collision frequencies are shown to be approximately 10 times less than at 200,000 ft. The electron-ion collision frequencies are approximately 100 times less than those for corresponding plasma-sheath locations at 200,000 ft. The reduced electron densities and collision frequencies at the higher altitude are indicative of the influence of nonequilibrium chemistry and initial density.

3.5 Determination of Important Chemical Reactions

The important chemical reactions involving charged species have been determined by comparison of the contribution of each reaction to the change in species concentration with distance along each streamline ($d\gamma_j^+/d\bar{x}$) This study was undertaken in an effort to truncate the chemical model currently in use and to determine the important electron-depletion and electron producing reactions. Comparisons were made for many points along each streamline in the plasma sheath. The value of ($d\gamma_j^+/d\bar{x}$) is given by Eq. (8)

$$\frac{d\gamma_j^+}{d\bar{x}} = \sum_{i=1}^{n} \beta_{ij} P_i X_i \qquad (8)$$

where $\bar{x}$ is the nondimensional distance x/ℓ

$$\beta_{ij} = \nu'_{ij} - \nu_{ij} \qquad (9)$$

$$P_i = \frac{\ell R_{fi}}{\rho u} \qquad (10), \qquad X_i = 1 - \frac{R_{ri}}{R_{fi}} \qquad (11)$$

and R_{fi} and R_{ri} are the forward and reverse rates of the ith reaction. The magnitude of ($d\gamma_j / d\bar{x}$) is indicative of the importance of the particular reaction for producing or depleting the species of interest. In this study a reaction was deemed important at a particular point along a streamline if the absolute value of its $P_i X_i$ product was within two orders of magnitude $P_i X_i$ at that point.

By use of the technique described above it was found that a negligible number of reactions could be dropped from the model currently in use. At some point or another within the flow field all but two of the reactions are important. The two reactions that could be eliminated from the model are the reactions:

$$e^- + N + O_2^+ \longrightarrow N + O_2$$

$$e^- + O + O_2^+ \longrightarrow O + O_2$$

This raises the always present question as to whether or not some of the possible reactions not included in the 64-reaction model might be important. This possibility is currently under investigation.

As suggested previously, in analyzing the streamtube results it was found that the species distributions through the flow field could be classified according to the location at which the streamtube crosses the shock. Table IV summarizes the various regions, the dominant ions, and the important reactions for that region. For a relatively short distance behind the translational shock there is in all cases what might be classed as a high-temperature, molecular ionization region. The dominant ions in this region are N_2^+, NO^+ and O_2^+. In the case of streamtubes that crossed the translational shock in the near normal portion, this molecular ionization region is followed by a high-temperature atomic ionization region. The dominant ions in the atomic ionization region are found to be N^+ and O^+. An intermediate-temperature, atomic and molecular ionization region was also found for which the dominant ions are N^+, NO^+ and O^+. This region immediately follows the high-temperature, molecular ionization region and is applicable to streamtubes that cross the translational shock between the near normal portion and the outer extremities. A low-temperature molecular ionization region was also found for which NO^+ is the dominant ion. Its location immediately follows the high-temperature, molecular ionization region for streamtubes crossing the outer extremities of the translational shock. The dominant chemical reactions for these three regions are distinctly different as illustrated by Table IV. The important electron-producing reactions are also shown in Table IV.

The dominant electron-depletion reactions were found to be the two-body dissociative-recombination reactions

$$NO^+ + e^- \longrightarrow N + O$$

$$N_2^+ + e^- \longrightarrow N + N$$

and the three-body electron-ion-recombination reactions

$$N^+ + e^- + e^- \longrightarrow N + e^-$$

$$O^+ + e^- + e^- \longrightarrow O + e^-$$

The two-body dissociative-recombination reactions are of approximately equal importance throughout the plasma sheath for these particular flight conditions. The three-body electron-ion recombination reactions become important beginning in the corner regions near the body. The reason for these reactions becoming important is the relatively large negative exponent of temperature appearing in the reaction rate constant and the rapid decrease in static temperature with the flow expansion.

The dominant charge-exchange reactions were determined for many locations within the plasma sheath. The particular reactions found to be important again vary with position in the plasma sheath. However, the following charge-exchange reactions are consistently important, although not necessarily the most important, at various plasma sheath locations.

$$O + N^+ \rightarrow N + O^+$$

$$O + N_2^+ \rightarrow N_2 + O^+$$

$$NO + N^+ \rightarrow N + NO^+$$

It is emphasized that specific plasma-sheath locations were found where other charge-exchange reactions given in Table II were equally important.

Similarly, the dominant ion-atom exchange reactions were determined for the entire plasma sheath. The following reactions were found to be the most consistently important.

$$N_2 + O^+ \longrightarrow N + NO^+$$

$$O + N_2^+ \longrightarrow N + NO^+$$

$$O + N_2^+ \longrightarrow NO + N^+$$

However, all of the ion-atom-exchange reactions were found to be important at some point within the plasma sheath.

The charge-exchange and ion-atom exchange reactions are important to the over-all chemical kinetics of the plasma. Both of these classes of reactions aid production of the molecular ion NO^+ which is then involved in the relatively fast dissociative-recombination reaction noted above.

Based on the model presented in Table II the important chemical reactions for various plasma sheath locations have been defined. Uncertainties in the values of the reaction rate constants utilized in these calculations have been discussed in Section 2. 3. It is important to note that the selected values of rate constant have a significant influence on the determination of the dominant reactions. It is felt, however, that the best available values have been used, and thus the results are as accurate as can be obtained at this time.

To illustrate the importance of utilizing a relatively complete chemical model for the calculation of the ionized flow field, the electron concentration along streamline 8 was recomputed for a truncated model Fig. 28, in which the charged species N^+, O^+, N_2^+ and O_2^+ and all reactions involving these species were deleted, only NO^+ being retained. As shown in Figure 28, the peak electron concentration for Model I is approximately an order of magnitude greater than that for Model II. Farther along the streamline the difference between the electron concentrations for the two models is reduced to a factor of approximately five. A similar comparison along the extremity streamlines for which N^+ and O^+ are not the dominant ions gives considerably better agreement between the streamline electron concentrations calculated using the different models. Thus, there are regions of the flow field for which the truncated model can be justifiably used to calculate the charged species concentrations.

4. CONCLUDING REMARKS

Nonequilibrium species concentrations along selected streamlines in the asymmetric Apollo plasma sheath have been presented. The species distributions have a defined pattern which is readily interpreted in terms of the local temperature, velocity, and density fields. With the exception of the body stagnation point and a relatively small region on the body surface, the plasma-sheath fluid was found to be in a nonequilibrium state for the trajectory points considered. The results indicate that the dominant ion in the early portion of the streamtube flow is, in general, N_2^+. At further distances along the higher initial temperature streamlines, N^+ and O^+ are dominant, whereas for the lower initial temperature streamlines NO^+ becomes dominant. For streamlines of intermediate static temperature, the ions NO^+, N^+ and O^+ are equally important. The calculations also illustrate the influence of initial density and local fluid velocity on the variation in species concentration with distance along the streamline. The streamlines of lower initial density were shown to require significantly longer flow distances to achieve maximum ionization. The dominant electron producing, electron depleting, charge exchange, and ion-atom exchange reactions are determined for many locations in the plasma sheath.

Contours of electron density in the forebody and near afterbody region have been presented for altitudes of 200,000 ft and 250,000 ft. For the 200,000 ft case, the maximum forebody electron density in the stagnation region was calculated to be approximately 5×10^{15} electrons/cm^3. In the windward corner region the electron density was on the order of 5×10^{13} electrons/cm^3 and in the leeward corner region, was approximately 5×10^{12} electrons/cm^3. Corresponding values of electron density for an altitude of 250,000 ft were found to approximately 50 times less.

Electron-neutral and electron-ion collision frequencies were also calculated along each streamline in the plane of symmetry. The solution for an altitude of 200,000 ft indicated a maximum electron-neutral collision frequency in excess of 1×10^{10} rad/sec in the forebody region. In the corner

region the electron-neutral collision frequencies were on the order of 5×10^9 rad/sec. The electron-ion collision frequencies in the forebody region were slightly less than the electron-neutral collision frequencies for the same region. The corner region values were approximately one-fifth the corresponding electron-neutral collision frequencies. Similar calculations were conducted for an altitude of 250,000 ft. For a given streamline the electron-neutral collision frequencies were found to be approximately an order of magnitude less than at 200,000 ft. The electron-ion collision frequencies were found to be approximately 1/100 those for corresponding plasma sheath locations at 200,000 ft.

The electron density distribution and the collision frequency distribution for two selected paths through the plasma sheath are presented. The peak electron densities and collision frequencies for these paths occur at a significant distance from the body. In addition, the values of the peak electron densities and collision frequencies are high emphasizing the importance of the inviscid flow field. From a communications viewpoint, it is important that the influence of ablation products and visous effects on the electromagnetic-propagation be compared to the influence of the inviscid flow field.

The attenuation for the propagation of one-dimensional plane waves along these two paths is presented. It must be emphasized that the accuracy of this electromagnetic-propagation calculation leading to the attenuation prediction is presently unknown. However, the implication of these results is that for the particular trajectory position and transmission paths selected, it would be exceedingly difficult to communicate with the craft at the currently available carrier frequencies.

REFERENCES

1. Bohachevsky, I. O. and Mates, R. E. , A Direct Method for Computation of Nonequilibrium Flows with Detached Shock Waves; Part II. Axisymmetric Blunt-Body at Angle of Attack, AIAA Paper No. 65-24, presented at the AIAA 2nd Aerospace Sciences Meeting (January 1965)

2. Bohachevsky, I. O. and Mates, R. E. , Axisymmetric Blunt Body at an Angle of Attack, Submitted for publication in AIAA Journal (August 1965)

3. Eschenroeder, A. Q. , Boyer, D. W. , and Hall, J. G. , Nonequilibrium Expansions of Air with Coupled Chemical Reactions, Phys. Fluids, Vol. 5, p. 615 (1962)

4. Lordi, J. A. , Mates, R. E. , and Moselle, J. R. , Computer Program for the Numerical Solution of Nonequilibrium Expansions of Reacting Gas Mixtures, Cornell Aeronautical Laboratory Report AD-1689-A-6 (June 1965)

5. Daiber, J. W. , Studies of Thermal Plasmas Associated with Hypersonic Re-entry Conditions, Cornell Aeronautical Laboratory First Semi-Annual Technical Summary Report, Contract Nonr 3960(00) (1962)

6. Hurle, I. R. and Russo, A. , Spectrum-Line Reversal Measurements of Free Electron and Coupled N_2 Vibrational Temperatures in Expansion Flows (to be published in J. Chem. Phys.)

7. Marrone, P. V. , Normal Shock Waves in Air: Equilibrium Composition and Flow Parameters for Velocities from 26,000 to 50,000 Ft/Sec Cornell Aeronautical Laboratory Report AG-1729-A-2 (1962)

8. Gilmore, F. , Equilibrium Composition and Thermodynamic Properties of Air to 24,000 °K, Rand Corp. Rept. RM-1543 (1955)

9. Marrone, P. V. , , Inviscid, Nonequilibrium Flow Behind Bow and Normal Shock Waves, Part I. General Analysis and Numerical Examples, Cornell Aeronautical Laboratory Report QM-1626-A-12 (I) (1963)

10. Hall, J. G. , Eschenroeder, A. Q. , and Marrone, P. V. , Inviscid Hypersonic Air Flows with Coupled Nonequilibrium Processes, J. Aero. Space Sci. , Vol. 29, p. 1038 (September 1962)

11. Eschenroeder, A. Q. , Daiber, J. W. , Golian, T. C. , and Hertzberg, A. , Shock Tunnel Studies of High Enthalpy Ionized Airflows, Cornell Aeronautical Laboratory Report AF-1500-A-1, AFOSR 3025 (July 1962)

12. Lin, S. C. , Neal, R. A. , and Fyfe, W. I. , Rate of Ionization Behind Shock Waves in Air; I. Experimental Results, Phys. Fluids, Vol. 5, p. 1633 (1962)

13. Makin, B. and Keck, J. C., Variational Theory of Three-Body Electron-Ion Recombination Rates, Phys. Rev. Letters, Vol. 11, p. 281 (1961)

14. Bortner, M. H., Chemical Kinetics in Reentry Flow Field, General Electric Co. Report R63SD63 (August 1963)

15. Bortner, M. H., The Effect of Errors in Rate Constants on Nonequilibrium Shock Layer Electron Density Calculations, Electromagnetic Effects of Re-entry, Edited by Rothman and Meltz, Pergamon Press, p. 74 (1961)

16. Bates, D. R., Kingston, A. E., and McWhirter, R. W. P., Recombination Between Electrons and Atomic Ions; II. Optically Thick Plasmas, Proc. Roy. Soc., A, Vol. 270, p. 155 (1962)

17. Hinnov, E. and Hirschberg, J. G., Electron-Ion Recombination in Dense Plasma, Phys. Rev., Vol. 125, p. 795 (1962)

18. Margenau, H., Conductions and Dispersion of Ionized Gases at High Frequencies, Phys. Rev., Vol. 69, p. 508 (1946)

19. Margenau, H., Conductivity of Plasmas to Microwaves, Phys. Rev., Vol. 109, p. 6 (1958)

20. Shkarofsky, I. P., Bachynski, M. P., and Johnson, T. W., Collision Frequency Associated with High Temperature Air and Scattering Cross-Sections of the Constituents, Electromagnetic Effects of Re-entry, Edited by W. Rotman, Pergamon Press (1961)

21. Spitzer, L. and Harm, R., Transport Phenomena in a Completely Ionized Gas., Phys. Rev., Vol. 89, p. 977 (1953)

22. Lin, S. C., A Rough Estimate of the Attenuation of Telemetering Signals Through the Ionized Gas Envelope Around a Typical Re-entry Missile, AVCO-Everett Res. Rept. 74 (February 1956)

23. Bein, G. P., Plane Wave Propagation at Arbitrary Angles of Incidence in Inhomogeneous, Lossy Plasmas. A High-Speed Computation Technique for Determining Complex Transmission and Reflection Coefficients, Cornell Aeronautical Laboratory, (to be submitted for publication in IEEE)

TABLE I
AIR REACTIONS FOR NEUTRAL SPECIES

$k_{F_i} = A_i T^{n_i} \exp(-\theta_i/T)$, cc/mole sec for T in °K

SPECIES CONSIDERED ARE: N_2, O_2, NO, N, O, Ar

REACTION	COLLISION PARTNER, M	A_i	n_i	θ_i
$N_2 + M \xrightarrow{k_{F_i}} 2N + M$	N_2	3.0×10^{21}	-1.5	113260
$N_2 + M \longrightarrow 2N + M$	N	1.5×10^{22}	-1.5	113260
$N_2 + M \longrightarrow 2N + M$	Ar, O, O_2, NO	9.9×10^{20}	-1.5	113260
$O_2 + M \longrightarrow 2O + M$	O_2	3.6×10^{21}	-1.5	59380
$O_2 + M \longrightarrow 2O + M$	O	2.1×10^{18}	-0.5	59380
$O_2 + M \longrightarrow 2O + M$	Ar, N, N_2, NO	1.2×10^{21}	-1.5	59380
$NO + M \longrightarrow N + O + M$	Ar, N_2, O_2, N, O	5.2×10^{21}	-1.5	75490
$N + O_2 \longrightarrow NO + N$		1.0×10^{12}	0.5	3120
$O + N_2 \longrightarrow NO + N$		5.0×10^{13}	0	38000
$NO + NO \longrightarrow N_2 + O_2$		4.8×10^{23}	-2.5	43000

TABLE II
AIR REACTIONS FOR IONIZED SPECIES

$k_{F_i} = A_i T^{n_i}$ $cm^3/mole\ sec$ (2 body reactions)

$k_{F_i} = A_i T^{n_i}$ $cm^6/mole^2\ sec$ (3 body reactions)

for T in °K

SPECIES CONSIDERED ARE: N_2^+, O_2^+, NO^+, N^+, O^+, and e^-

REACTION	M	A_i	n_i
DISSOCIATIVE RECOMBINATION REACTIONS			
$e^- + NO^+ \longrightarrow N + O$		1.8×10^{21}	-1.5
$e^- + N_2^+ \longrightarrow N + N$		1.0×10^{21}	-1.5
$e^- + O_2^+ \longrightarrow O + O$		1.0×10^{21}	-1.5
THREE-BODY RECOMBINATION REACTIONS			
$e^- + NO + NO^+ \longrightarrow N_2 + O_2$		1.0×10^{24}	-2.5
$e^- + N + M^+ \longrightarrow N + M$		6.0×10^{24}	-2.5
$e^- + O + M^+ \longrightarrow O + M$		6.0×10^{24}	-2.5
$e^- + N_2 + M^+ \longrightarrow N_2 + M$	NO, N, O, O_2, N_2	2.22×10^{26}	-2.5
$e^- + O_2 + M^+ \longrightarrow O_2 + M$		8.8×10^{26}	-2.5
$e^- + NO + M^+ \longrightarrow NO + M$		1.31×10^{28}	-2.5
$e^- + e^- + M^+ \longrightarrow e^- + M$		8.3×10^{39}	-4.5
CHARGE-EXCHANGE REACTIONS			
$O + M^+ \longrightarrow M + O^+$	N, N_2	7.8×10^{11}	0.5
$N + N_2^+ \longrightarrow N_2 + N^+$			
$O_2 + M^+ \longrightarrow M + O_2^+$	O, N, N_2		
$NO + M^+ \longrightarrow M + NO^+$	O, N, O_2, N_2		
ION-ATOM EXCHANGE REACTIONS			
$O + N_2^+ \longrightarrow N + NO^+$		7.8×10^{11}	0.5
$N + O_2^+ \longrightarrow O + NO^+$			
$N_2 + O^+ \longrightarrow N + NO^+$			
$N_2 + O_2^+ \longrightarrow NO + NO^+$			
$O_2 + N^+ \longrightarrow NO + O^+$			
$O_2 + N^+ \longrightarrow O + NO^+$			
$O_2 + N_2^+ \longrightarrow NO + NO^+$			
$NO + O^+ \longrightarrow N + O_2^+$			
$NO + N^+ \longrightarrow O + N_2^+$			
$NO + N^+ \longrightarrow N_2 + O^+$			

TABLE III

ESTIMATED RATE CONSTANT UNCERTAINTY

REACTIONS	RATE CONSTANT	RATE CONSTANT EVALUATED AT			REF.
		290°K	2000°K	4000°K	
(A) ELECTRON DEPLETION					
(1) $NO^+ + e^- \longrightarrow N + O$	(1) $k = 1.8 \times 10^{21}T^{-1.5}$ cm^3/mole sec $k = 2.0 \times 10^{19\pm2}T^{-1.0}$ cm^3/mole sec	(1) 3.6×10^{17} $6.9 \times 10^{16\pm2}$	(1) 2.0×10^{16} $1.0 \times 10^{16\pm2}$	(1) 7.1×10^{15} $5.0 \times 10^{16\pm2}$	12 14
(2) $N_2^+ + e^- \longrightarrow N + N$	(2) $k = 1.0 \times 10^{21}T^{-1.5}$ cm^3/mole sec $k = 5.0 \times 10^{18\pm1}T^{-0.5}$ cm^3/mole sec	(2) 2.0×10^{17} $2.9 \times 10^{17\pm1}$	(2) 1.1×10^{16} $1.1 \times 10^{17\pm1}$	(2) 3.9×10^{15} $8.0 \times 10^{16\pm1}$	11 14
(3) $O^+ + e^- + e^- \longrightarrow O + e^-$	(3) $k = 8.3 \times 10^{39}T^{-4.5}$ cm^6/mole^{2}sec $k = 4.0 \times 10^{21\pm1}T^{-1}$ cm^6/mole^{2}sec	(3) 6.9×10^{28} $1.4 \times 10^{19\pm1}$	(3) 6.4×10^{24} $2.0 \times 10^{18\pm1}$	(3) 2.9×10^{23} $1.0 \times 10^{18\pm1}$	13 14
(B) CHARGE EXCHANGE					
(4) $O + N^+ \longrightarrow N + O^+$	(4) $k = 7.8 \times 10^{11}T^{0.5}$ cm^3/mole sec $k = 5.0 \times 10^{13\pm2}T^{-0.5}$ cm^3/mole sec	(4) 1.3×10^{13} $2.9 \times 10^{12\pm2}$	(4) 3.5×10^{13} $1.1 \times 10^{12\pm2}$	(4) 5.0×10^{13} $7.8 \times 10^{11\pm2}$	11 14
(C) ION-ATOM EXCHANGE					
(5) $N_2 + O^+ \longrightarrow N + NO^+$	(5) $k = 7.8 \times 10^{11}T^{0.5}$ cm^3/mole sec $k = 1.0 \times 10^{13\pm2}T^{-0.5}$ cm^3/mole sec	(5) 1.3×10^{13} $5.9 \times 10^{11\pm2}$	(5) 3.5×10^{13} $2.2 \times 10^{11\pm2}$	(5) 5.0×10^{13} $1.6 \times 10^{11\pm2}$	11 14
(6) $O + N_2^+ \longrightarrow N + NO^+$	(6) $k = 7.8 \times 10^{11}T^{0.5}$ cm^3/mole sec $k = 1.0 \times 10^{14\pm2}T^{-0.5}$ cm^3/mole sec	(6) 1.3×10^{13} $5.9 \times 10^{12\pm2}$	(6) 3.5×10^{13} $2.2 \times 10^{12\pm2}$	(6) 5.0×10^{13} $1.6 \times 10^{12\pm2}$	11 14

TABLE IV

SUMMARY OF NONEQUILIBRIUM IONIZATION CALCULATIONS

CLASSIFICATION OF REGION	LOCATION	DOMINANT IONS	IMPORTANT CHEMICAL REACTIONS
I. HIGH-TEMPERATURE, MOLECULAR IONIZATION REGION	RELATIVELY SHORT DISTANCE BEHIND TRANSLATIONAL SHOCK FOR ALL STREAMLINES CONSIDERED (SEE FIG. 1)	N_2^+, NO^+, O_2^+	(a) $e^- + N_2 \rightarrow e^- + e^- + N_2^+$ (b) $O + N_2^+ \rightarrow N + NO^+$ (c) $N_2 + N^+ \rightarrow N + N_2^+$ (d) $N_2 + O_2^+ \rightarrow NO + NO^+$ (e) $N_2 + NO \rightarrow e^- + NO + N_2^+$
II. HIGH-TEMPERATURE, ATOMIC IONIZATION REGION	REGION IMMEDIATELY FOLLOWING MOLECULAR IONIZATION REGION FOR STREAMTUBES THAT CROSS NEAR NORMAL PORTIONS OF TRANSLATIONAL SHOCK. (FOR EXAMPLE, STREAMLINES 5 AND 8).	N^+, O^+	(a) $e^- + N \rightarrow e^- + e^- + N^+$ (b) $O + N^+ \rightarrow N + O^+$ (c) $e^- + O \rightarrow e^- + e^- + O^+$ (d) $N_2 + O^+ \rightarrow NO + N^+$
III. INTERMEDIATE-TEMPERATURE, ATOMIC AND MOLECULAR IONIZATION REGION	REGION IMMEDIATELY FOLLOWING MOLECULAR IONIZATION REGION FOR STREAMTUBES THAT CROSS TRANSLATIONAL SHOCK BETWEEN NORMAL PORTION AND OUTER EXTREMITIES (FOR EXAMPLE, STREAMLINES 3 AND 12).	N^+, NO^+, N_2^+, O^+	(a) $O + N^+ \rightarrow N + O^+$ (b) $N_2 + O^+ \rightarrow N + NO^+$ (c) $O + N_2^+ \rightarrow NO + N^+$ (d) $e^- + N \rightarrow e^- + e^- + N^+$ (e) $O + N_2^+ \rightarrow N + NO^+$
IV. LOW-TEMPERATURE, MOLECULAR IONIZATION REGION	REGION IMMEDIATELY FOLLOWING MOLECULAR IONIZATION REGION FOR STREAMTUBES THAT CROSS TRANSLATIONAL SHOCK AT OUTER EXTREMITIES (FOR EXAMPLE, STREAMLINE 14).	NO^+	(a) $N_2 + O_2^+ \rightarrow NO + NO^+$ (b) $O + N_2^+ \rightarrow N + NO^+$ (c) $O + N_2^+ \rightarrow NO + NO^+$ (d) $NO + NO \rightarrow NO + NO^+ + e^-$

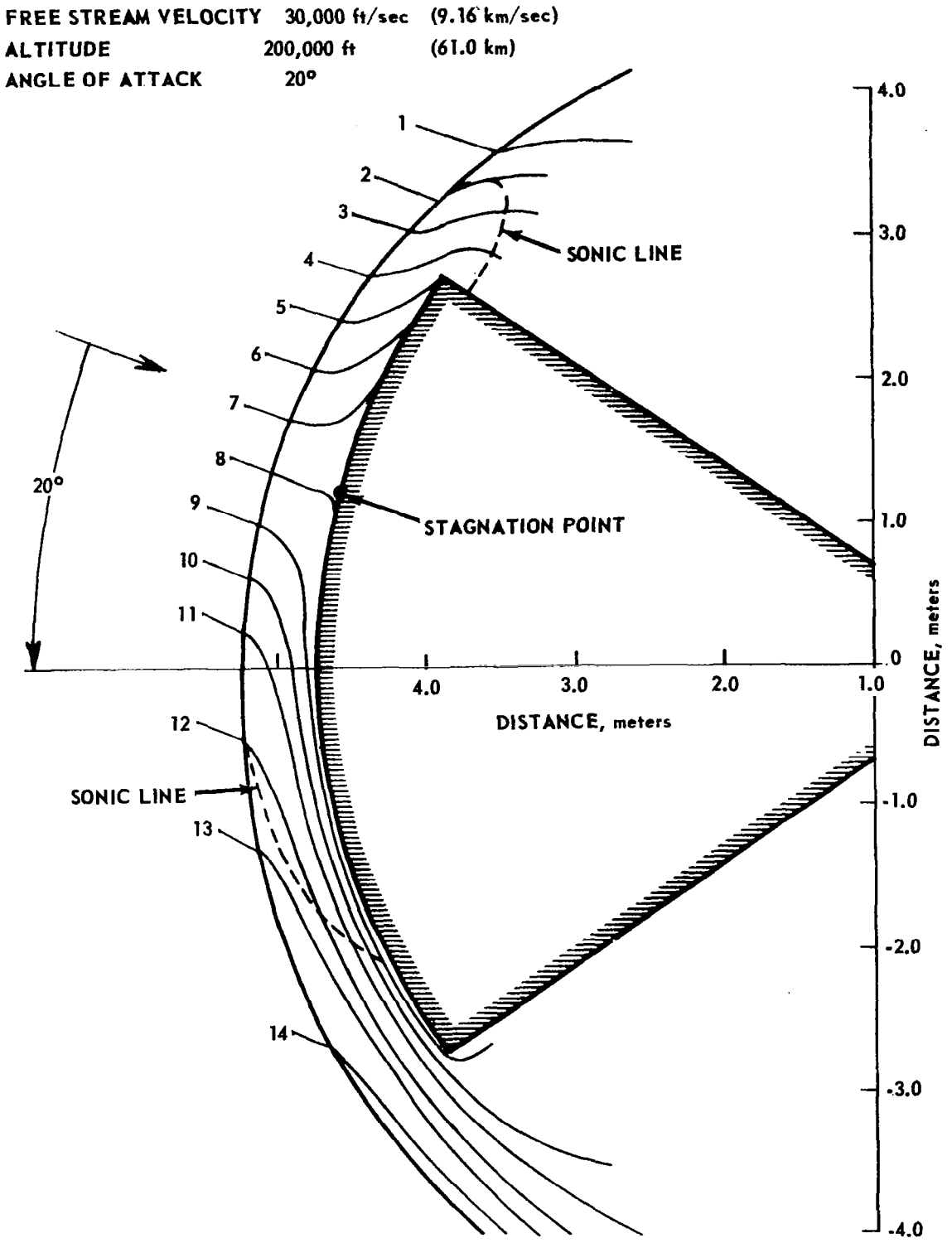

FIGURE 1 STREAMLINE PATTERN IN THE PLANE OF SYMMETRY

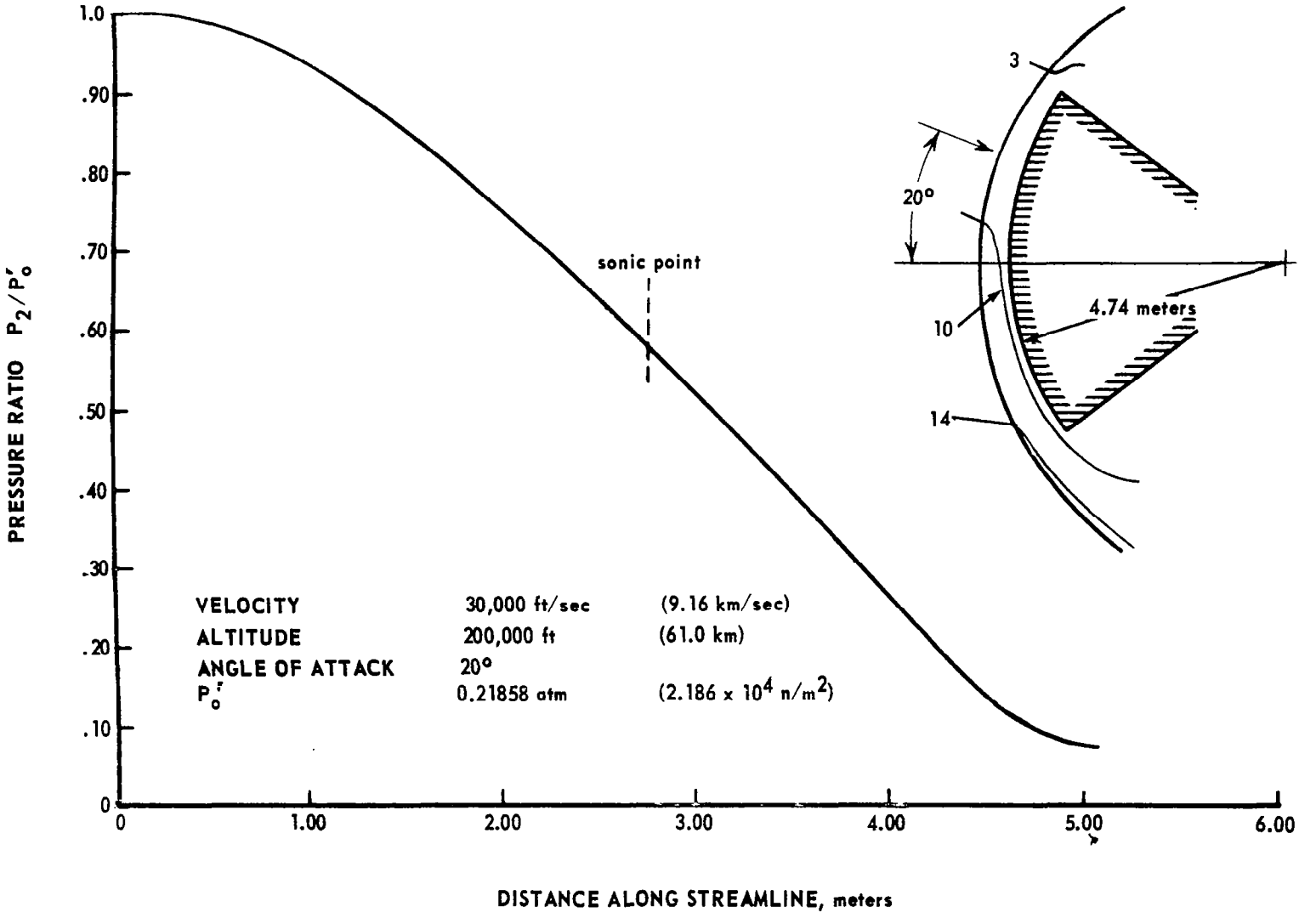

FIGURE 2 PRESSURE DISTRIBUTION IN PLANE OF SYMMETRY FOR STREAMLINE 10

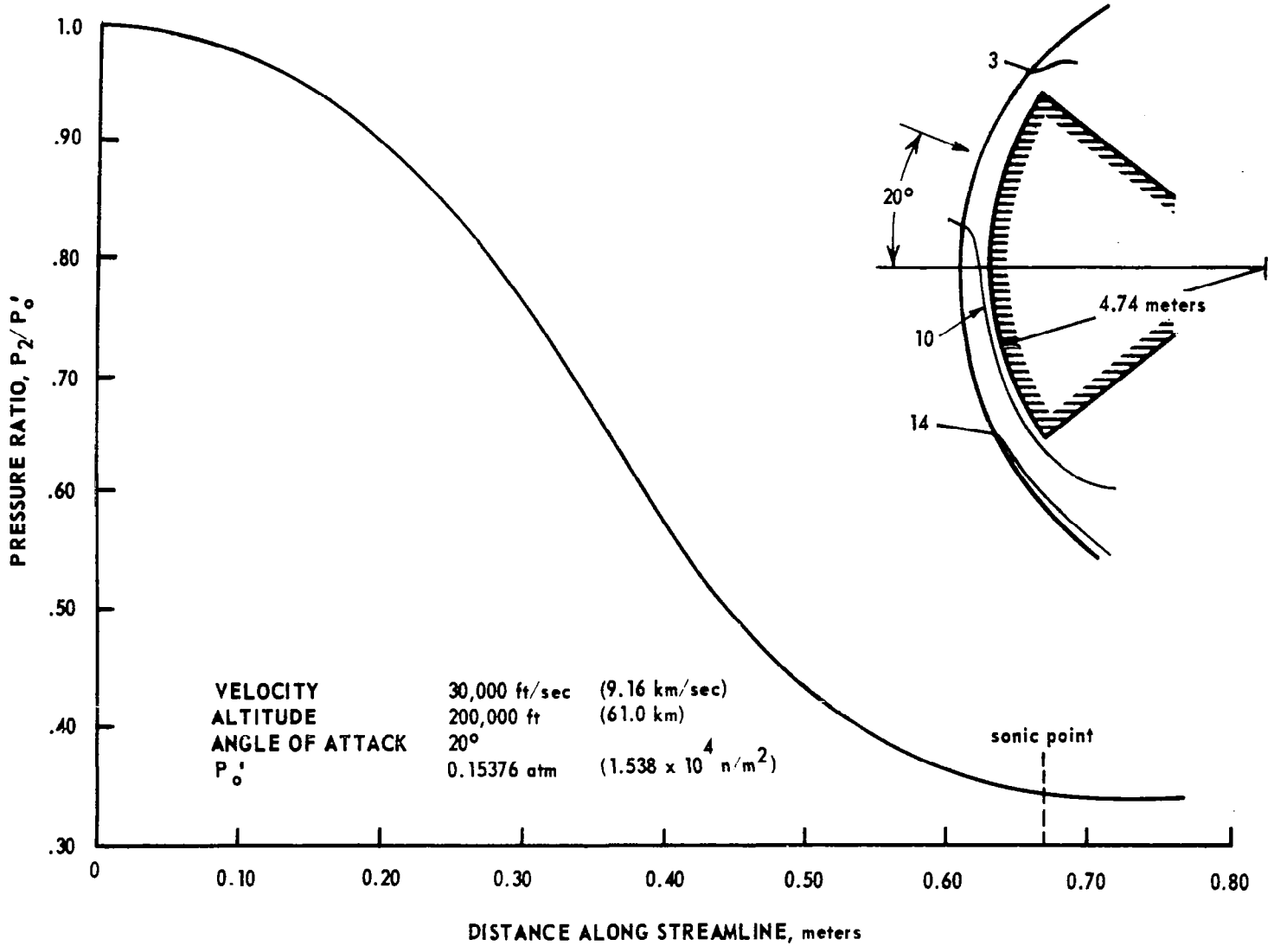

FIGURE 3 PRESSURE DISTRIBUTION IN PLANE OF SYMMETRY FOR STREAMLINE 3

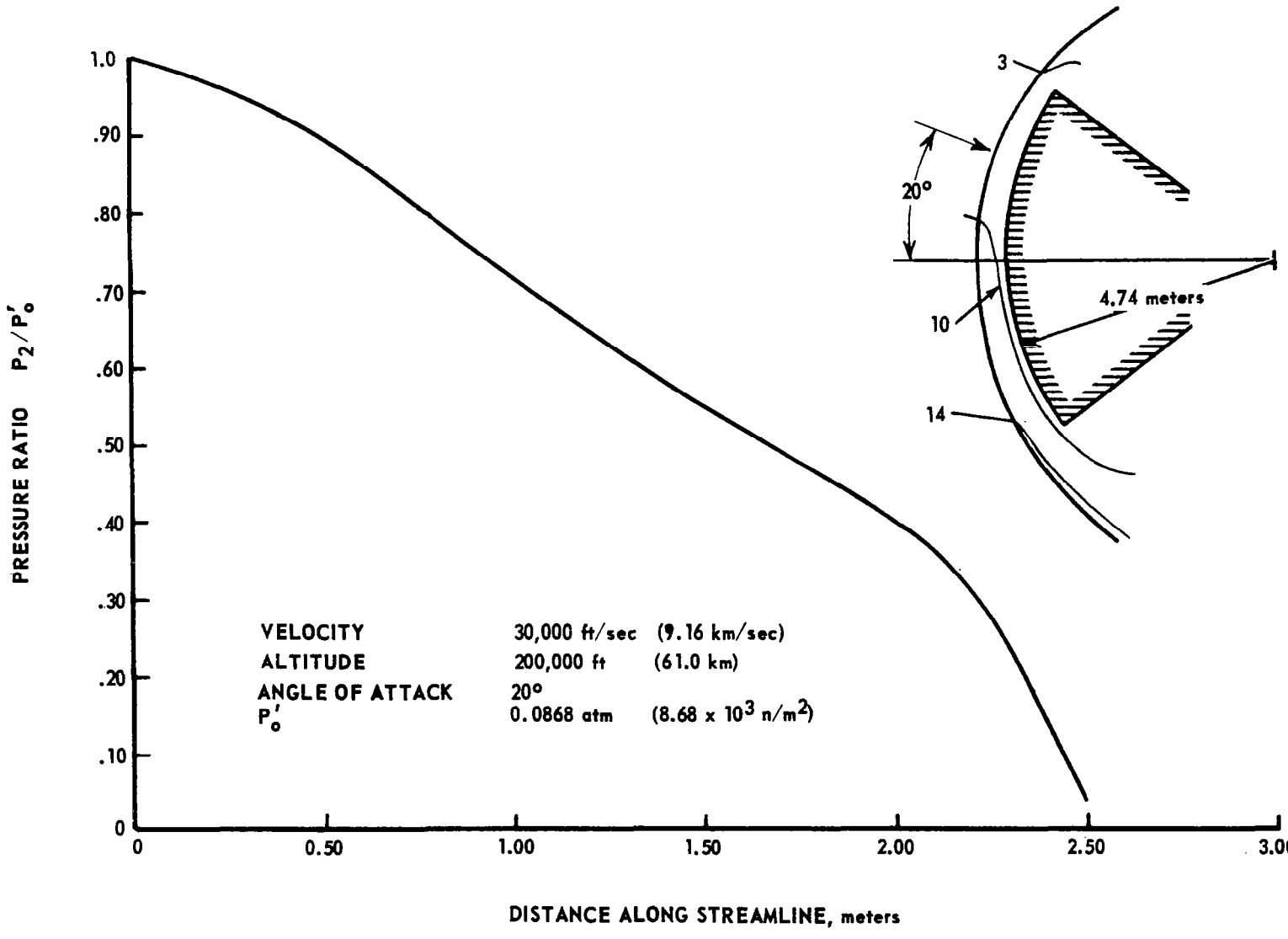

FIGURE 4 PRESSURE DISTRIBUTION IN PLANE OF SYMMETRY FOR STREAMLINE 14

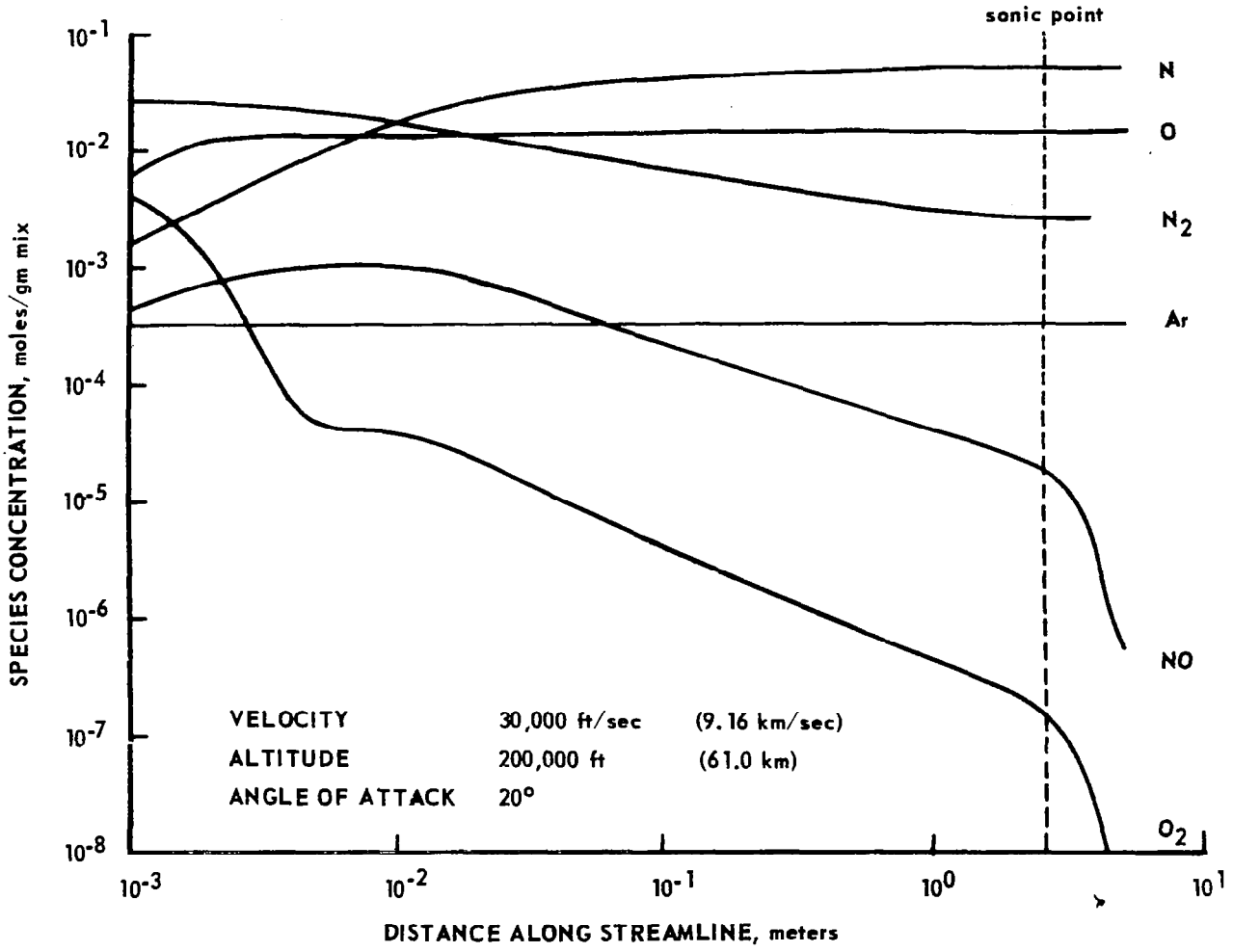

FIGURE 5 NONEQUILIBRIUM SPECIES DISTRIBUTION ALONG STREAMLINE 10 IN PLANE OF SYMMETRY

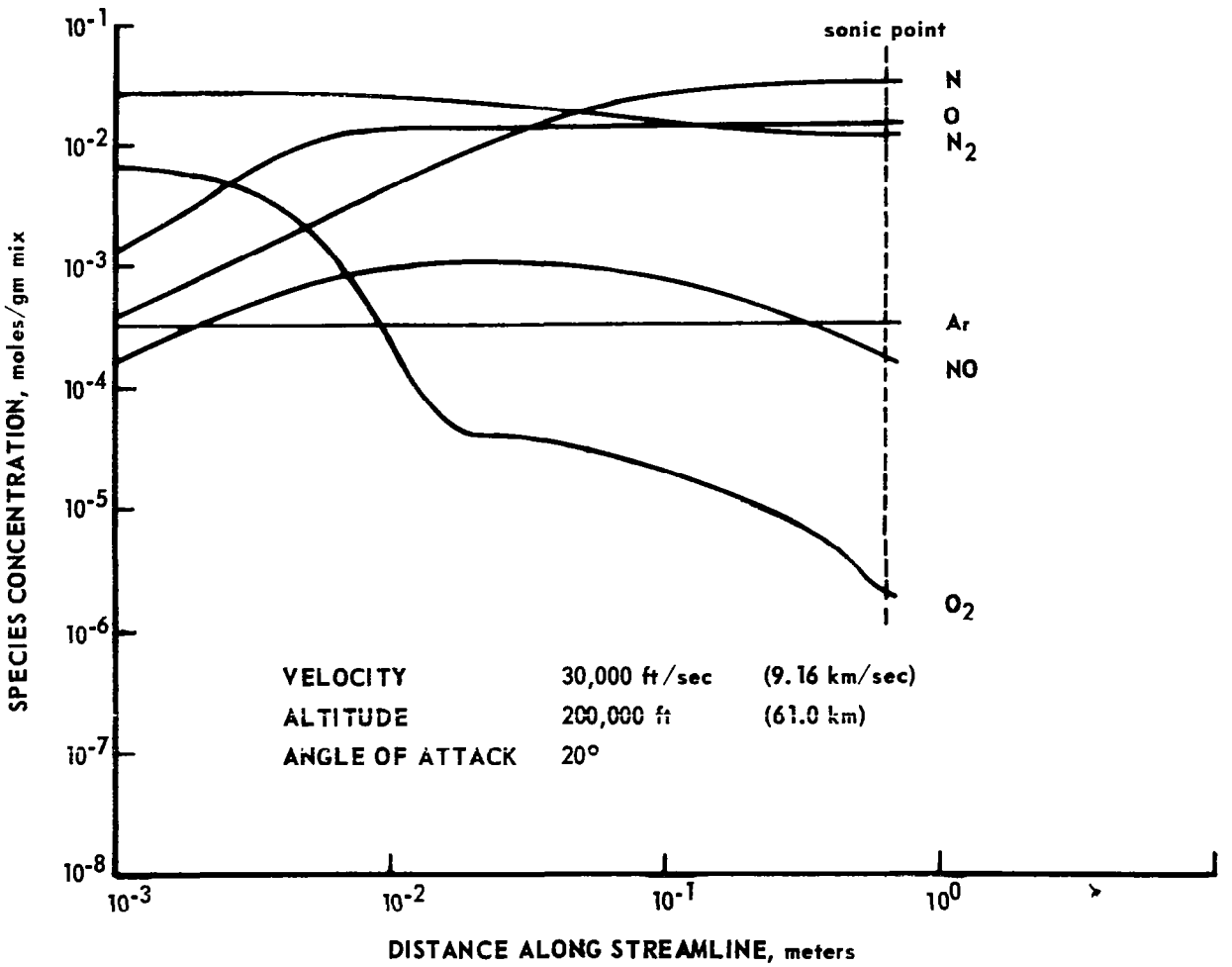

FIGURE 6 NONEQUILIBRIUM SPECIES DISTRIBUTION ALONG STREAMLINE 3 IN PLANE OF SYMMETRY

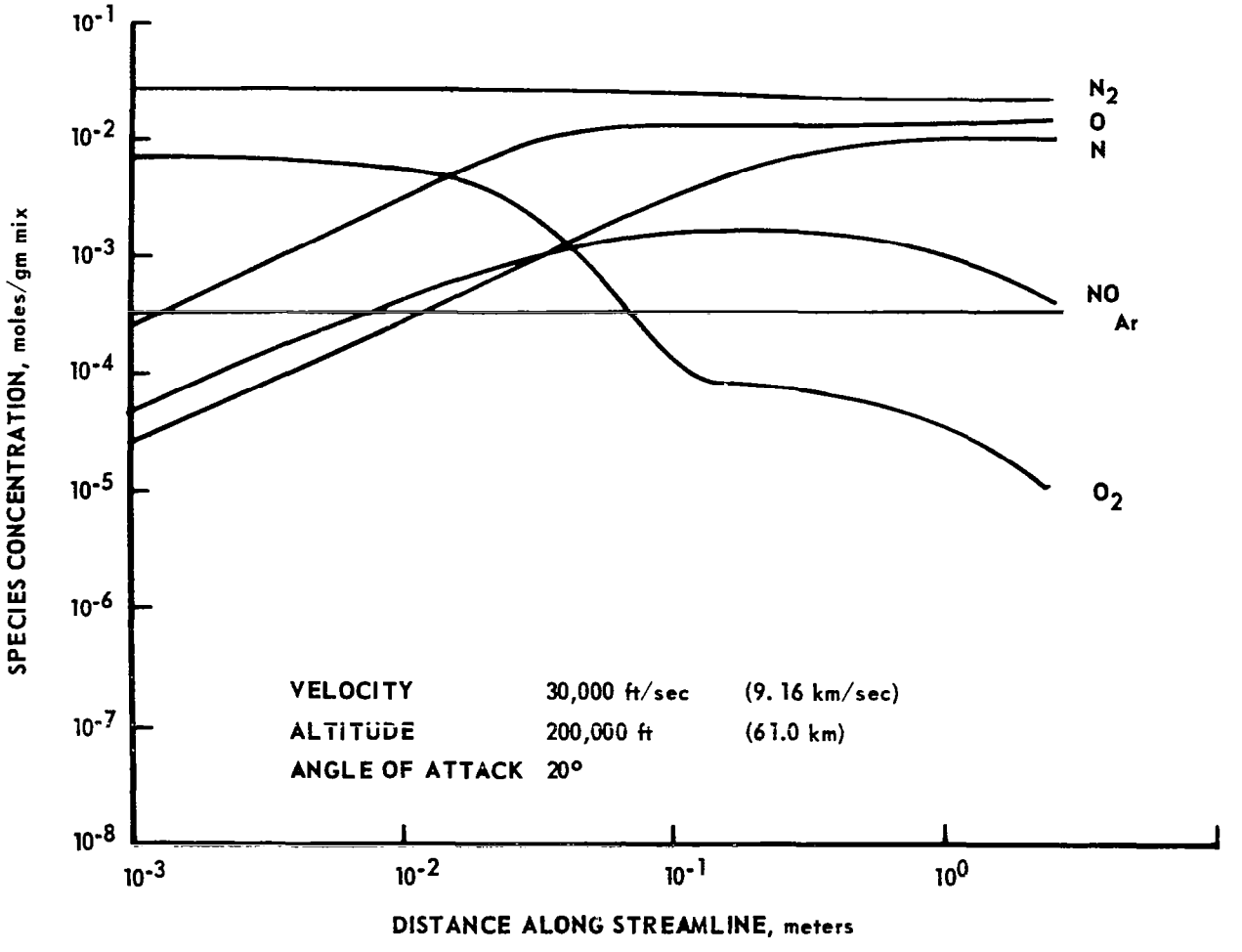

FIGURE 7 NONEQUILIBRIUM SPECIES DISTRIBUTION ALONG STREAMLINE 14 IN PLANE OF SYMMETRY

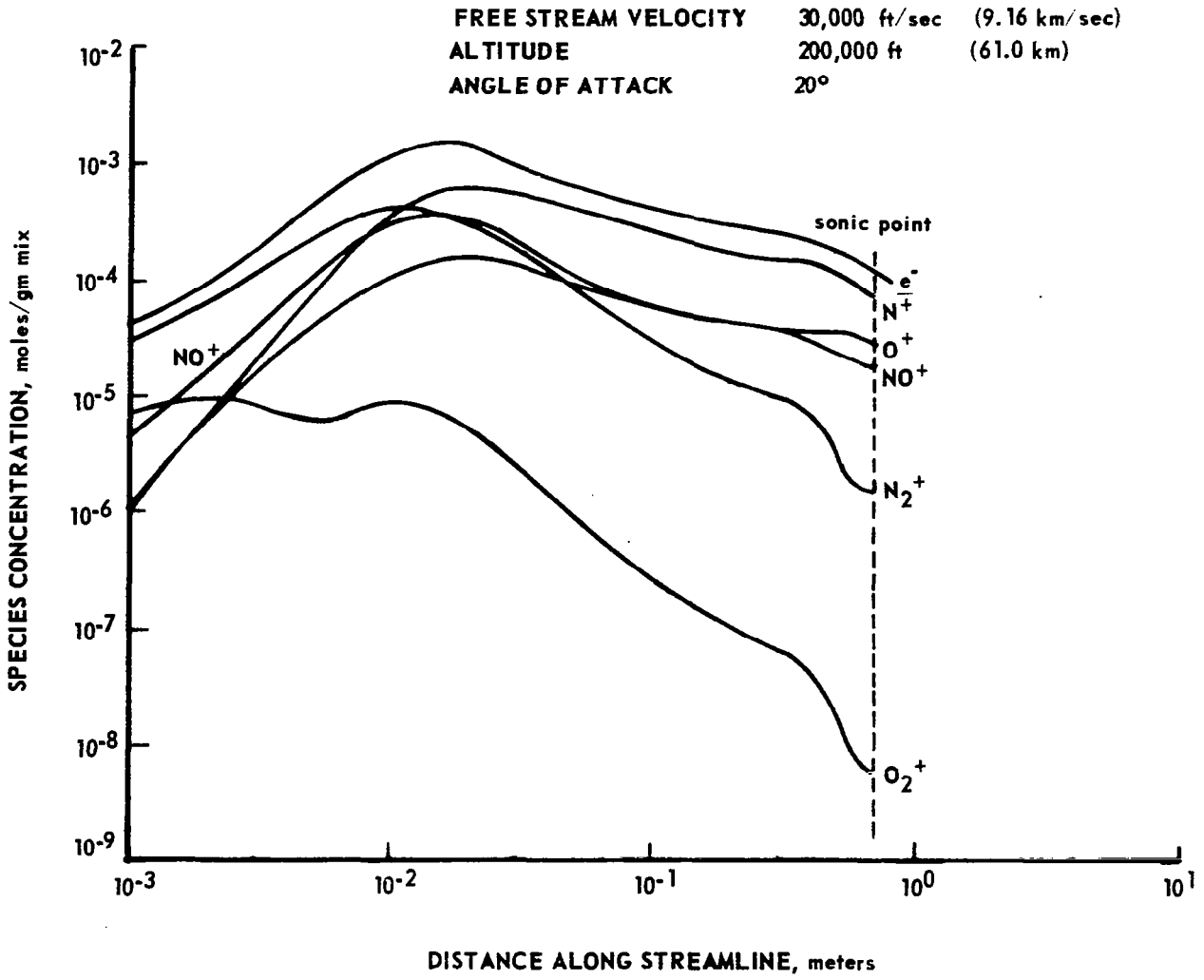

FIGURE 8 NONEQUILIBRIUM SPECIES DISTRIBUTION ALONG STREAMLINE 5 IN PLANE OF SYMMETRY

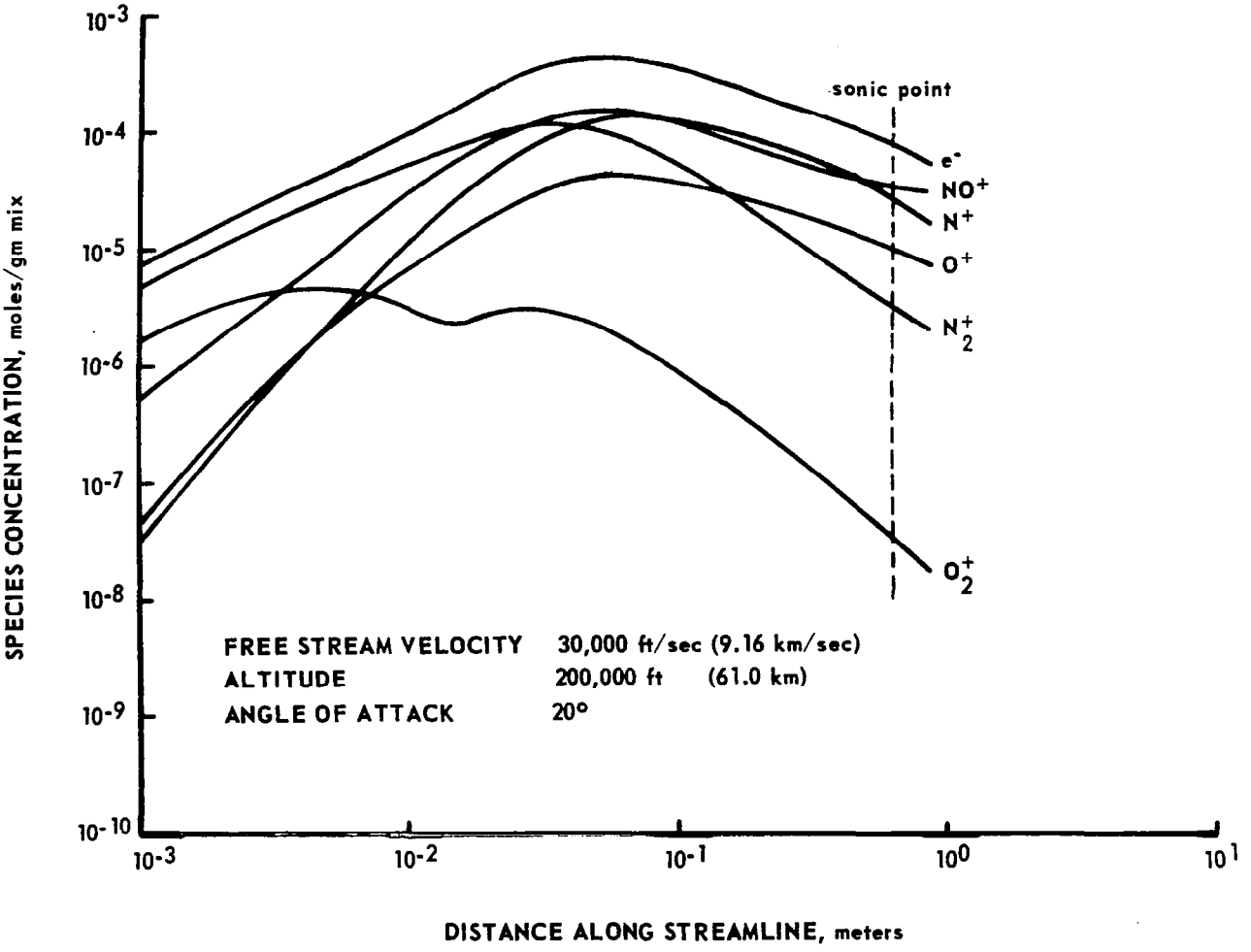

FIGURE 9 NONEQUILIBRIUM SPECIES DISTRIBUTION ALONG STREAMLINE 3 IN PLANE OF SYMMETRY

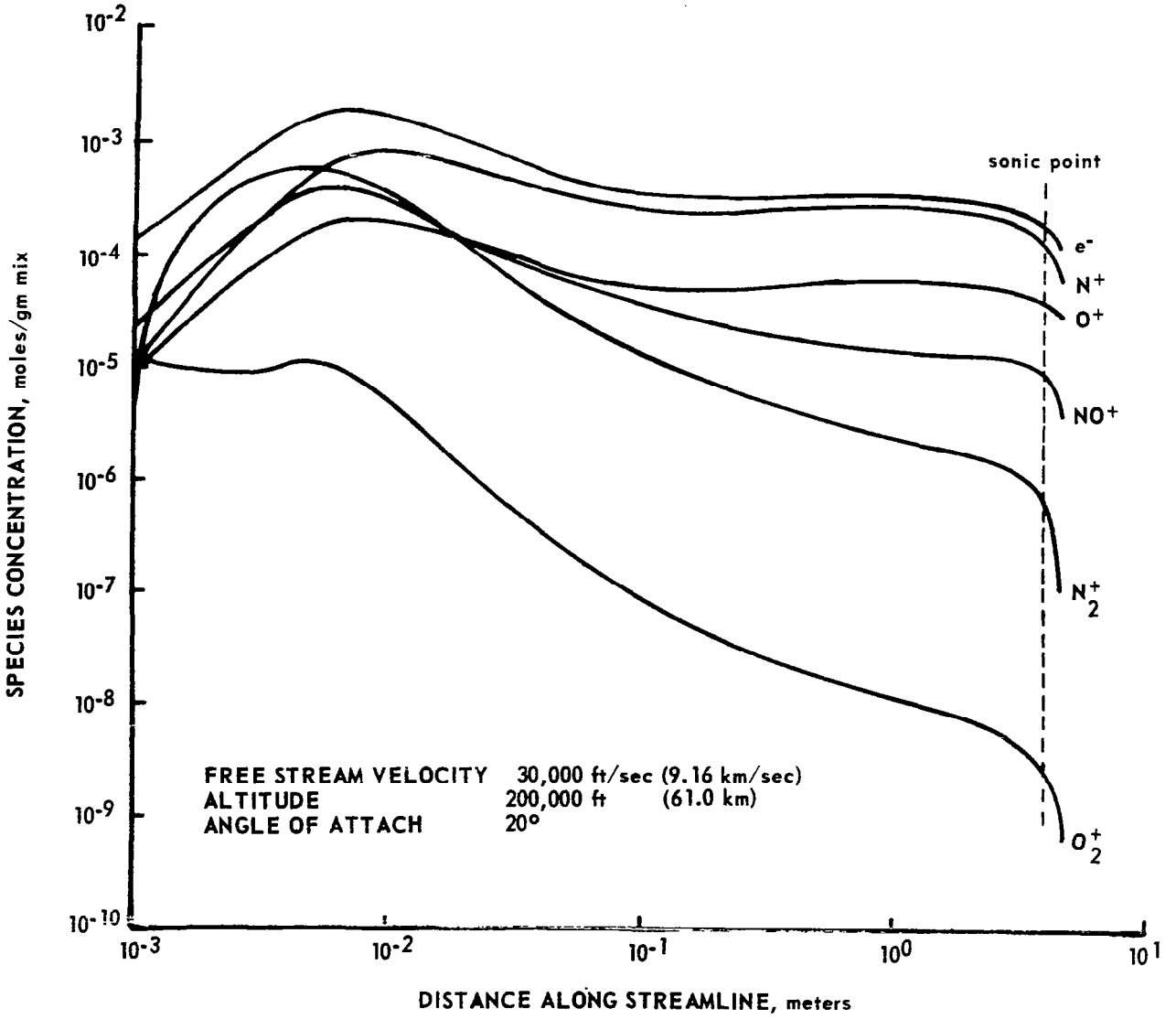

FIGURE 10 NONEQUILIBRIUM SPECIES DISTRIBUTION ALONG STREAMLINE 8 IN PLANE OF SYMMETRY

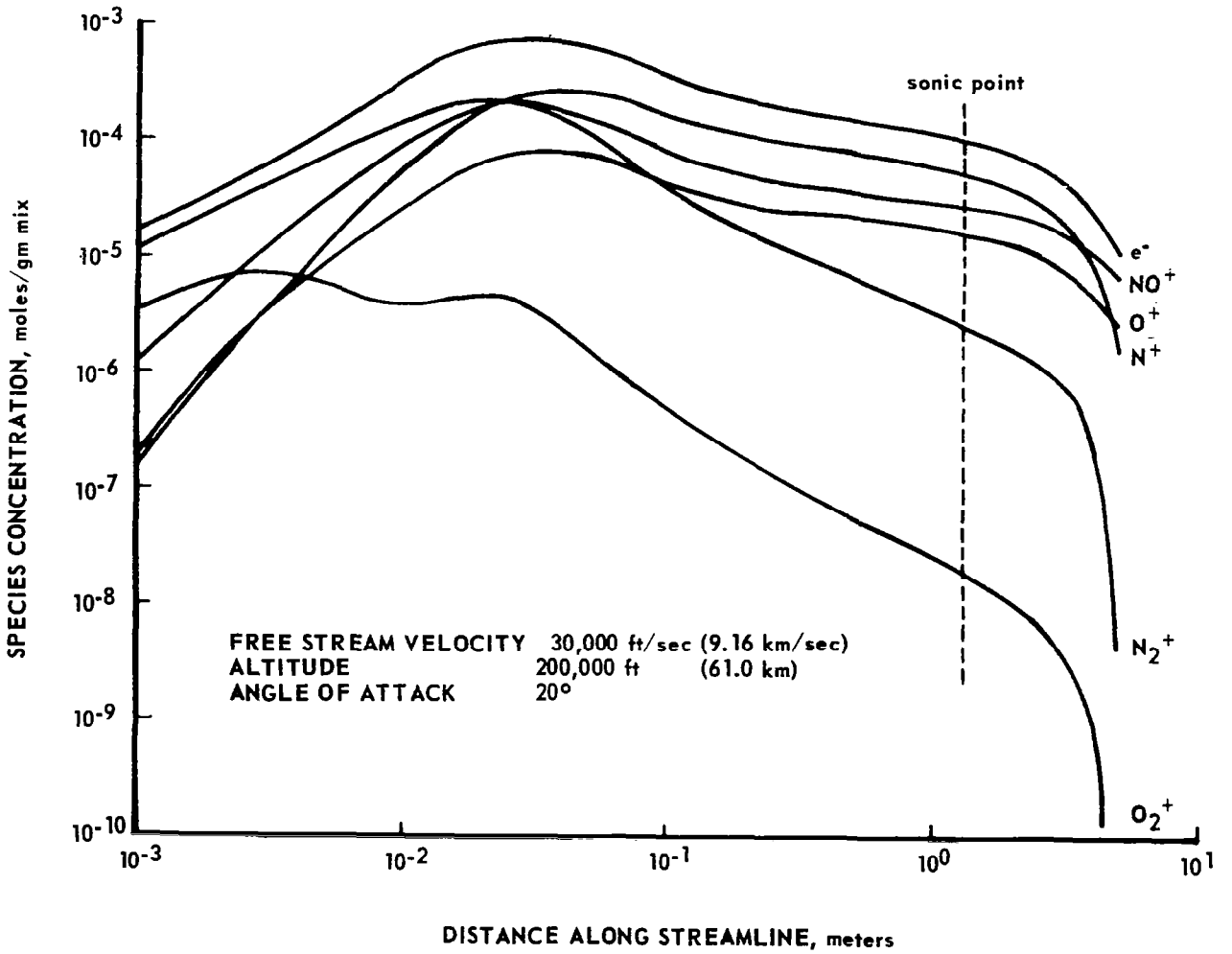

FIGURE 11 NONEQUILIBRIUM SPECIES DISTRIBUTION ALONG STREAMLINE 12 IN PLANE OF SYMMETRY

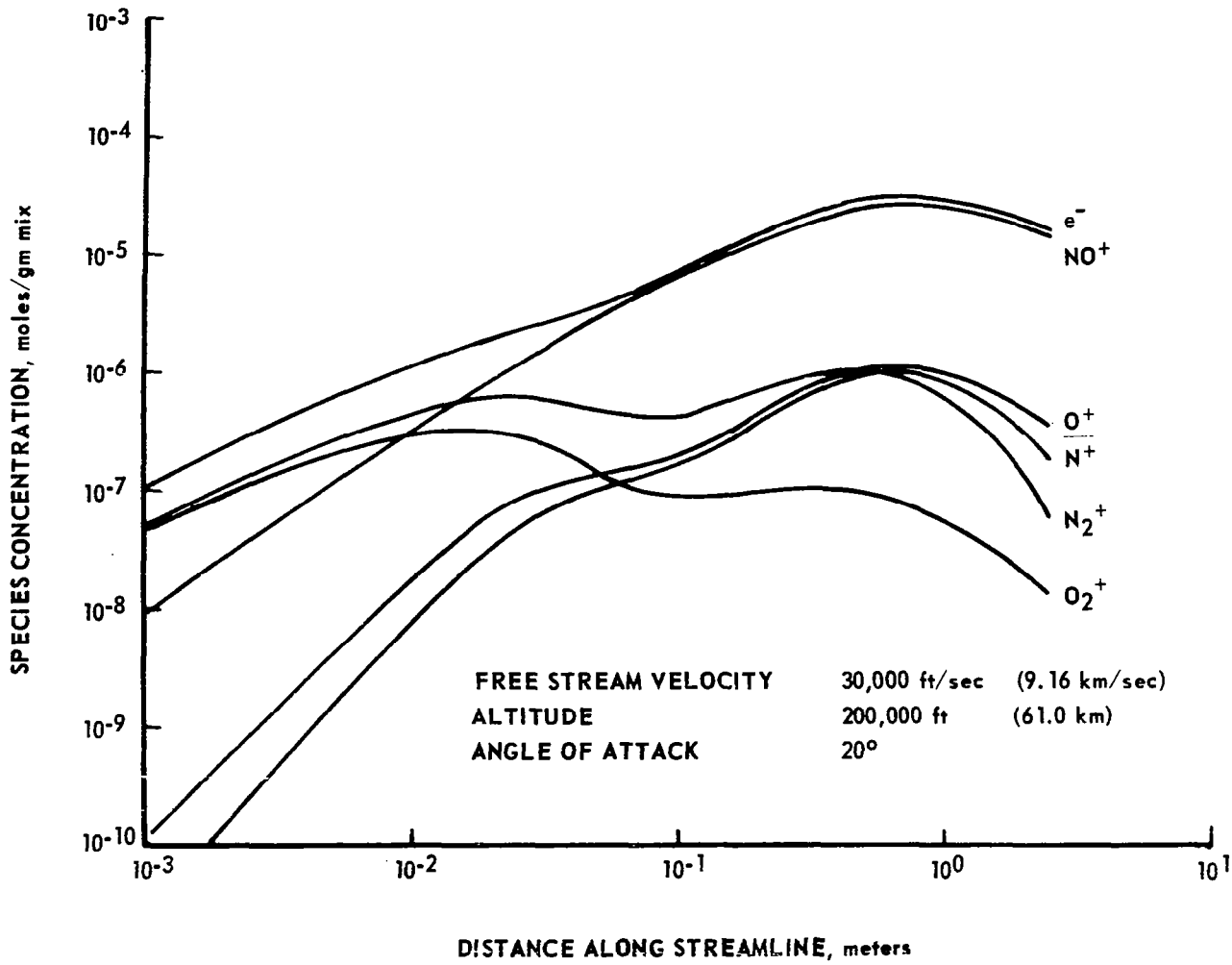

FIGURE 12 NONEQUILIBRIUM SPECIES DISTRIBUTION ALONG STREAMLINE 14 IN PLANE OF SYMMETRY

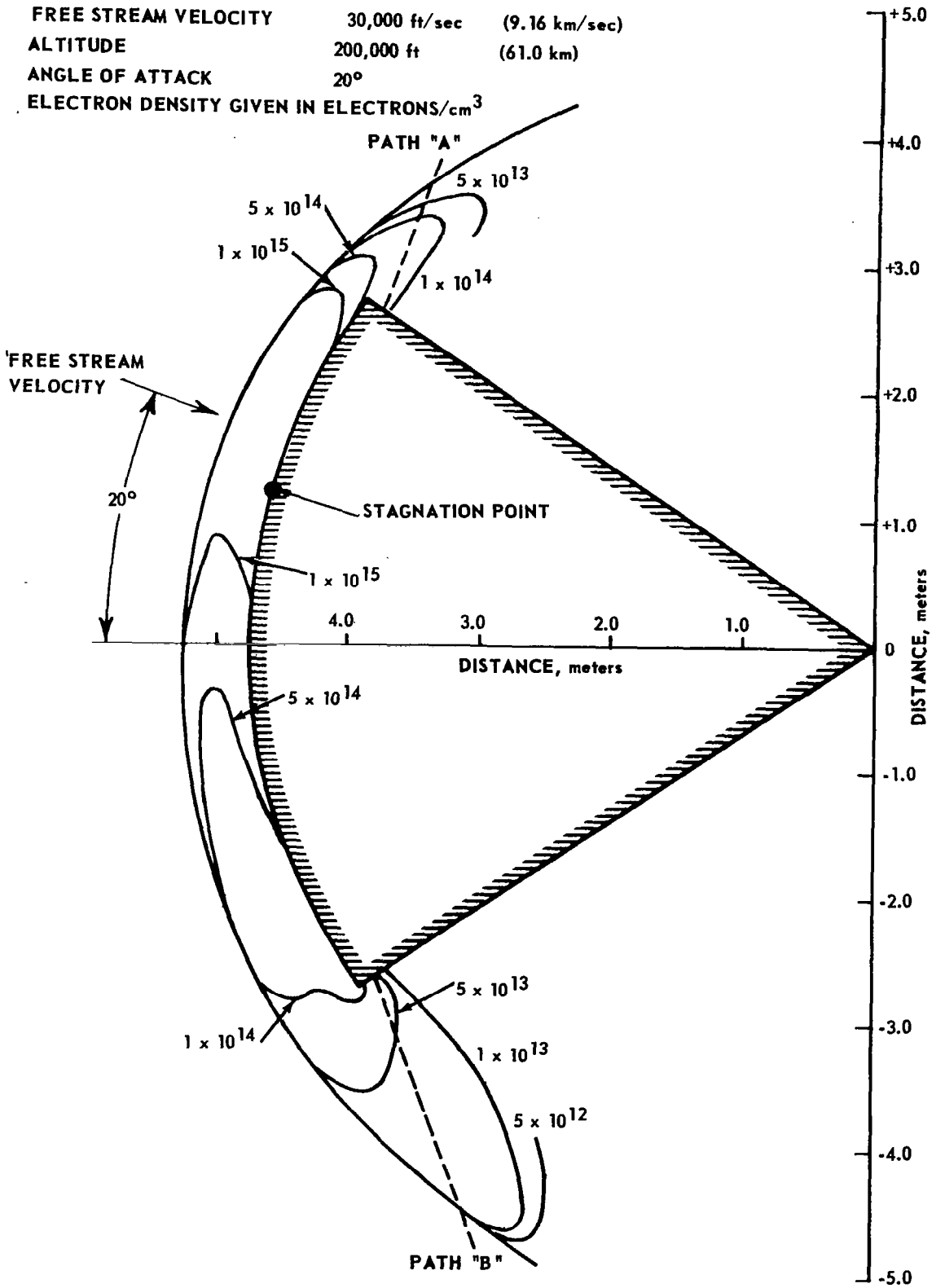

FIGURE 13 ELECTRON DENSITY DISTRIBUTION IN PLANE OF SYMMETRY

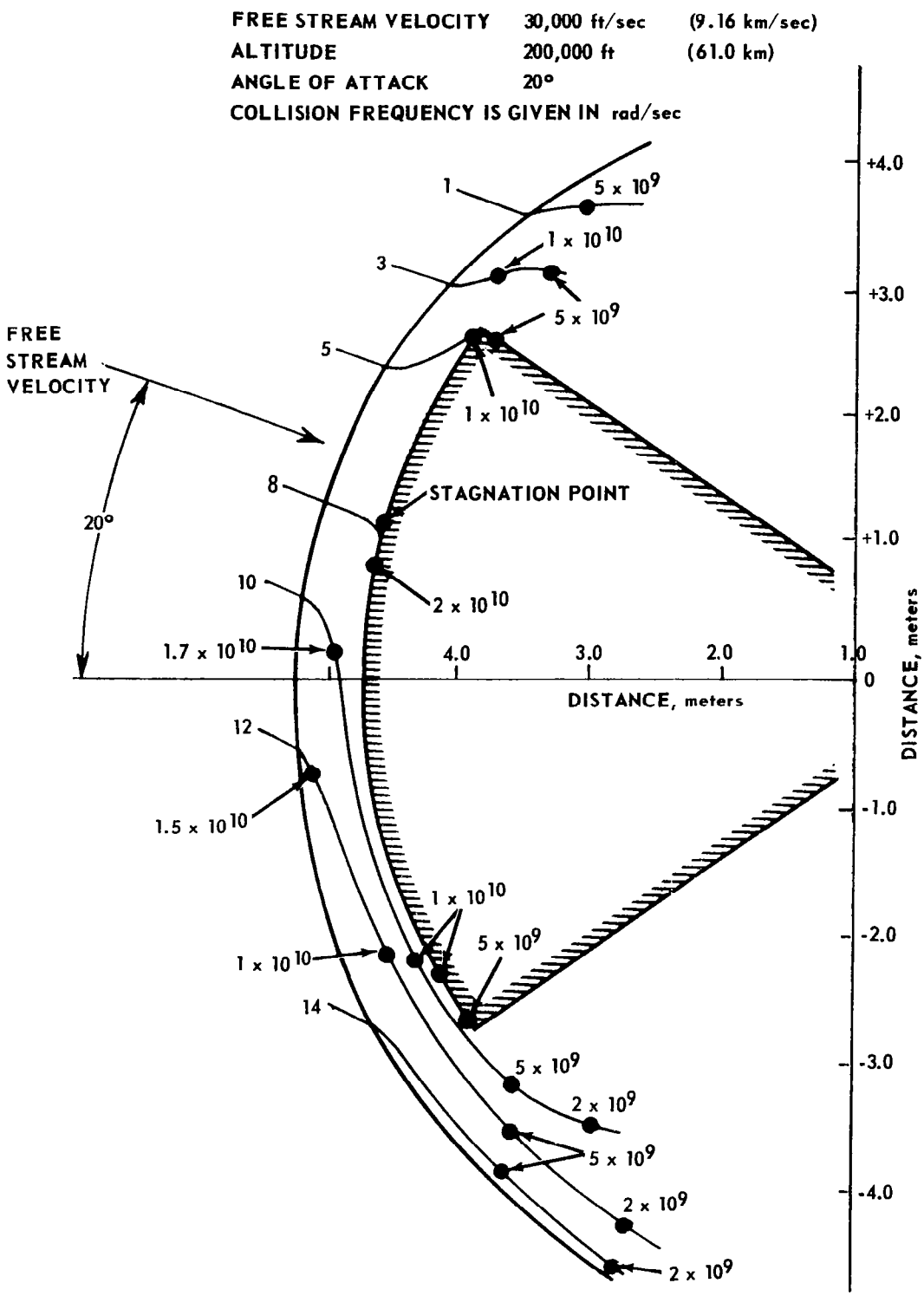

FIGURE 14 ELECTRON-NEUTRAL COLLISION FREQUENCY (ν) IN PLANE OF SYMMETRY

FREE STREAM VELOCITY 30,000 ft/sec (9.16 km/sec)
ALTITUDE 200,000 ft (61.0 km)
ANGLE OF ATTACK 20°
COLLISION FREQUENCY IS GIVEN IN rad/sec

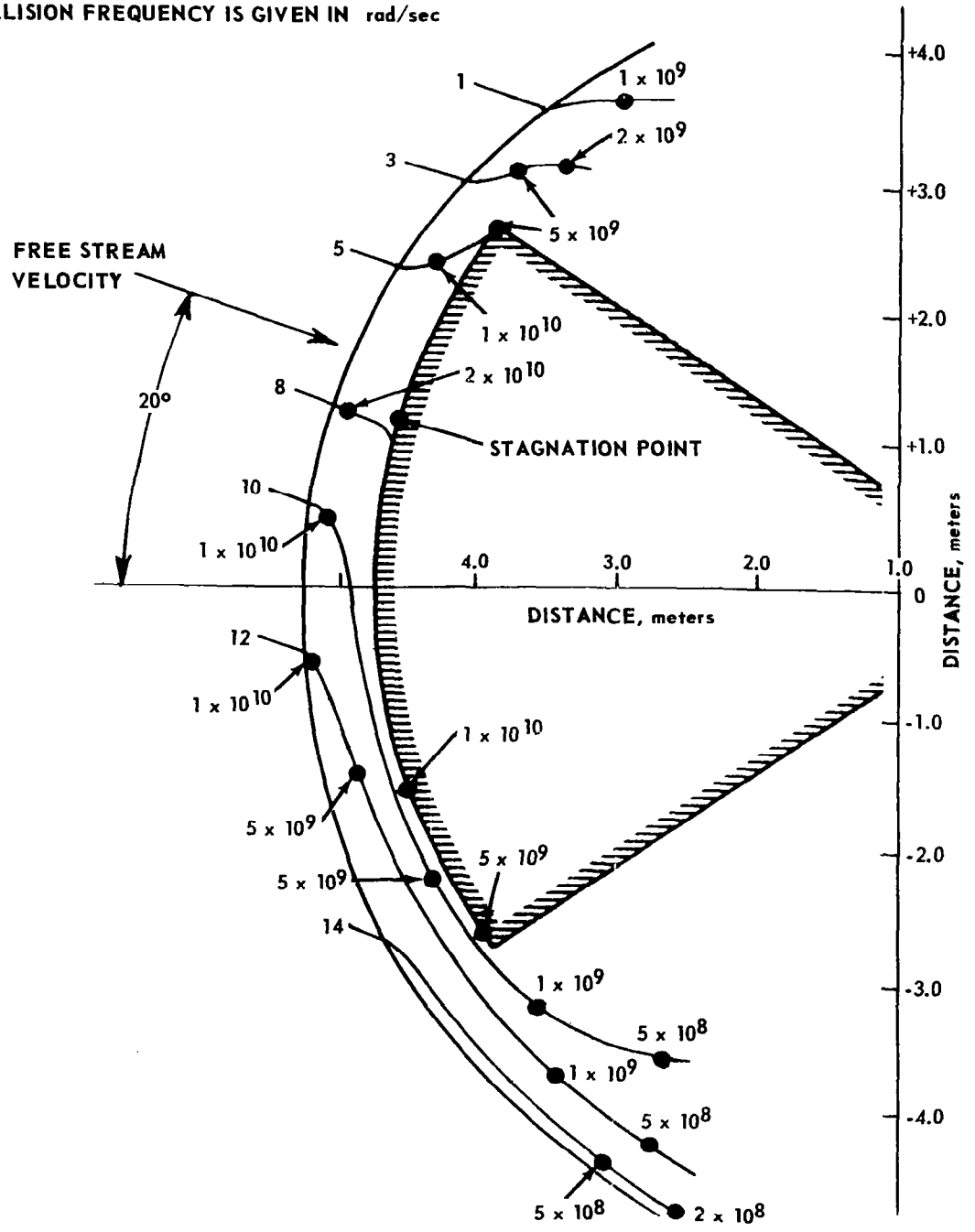

FIGURE 15 ELECTRON-ION COLLISION FREQUENCY (ν^+) IN PLANE OF SYMMETRY

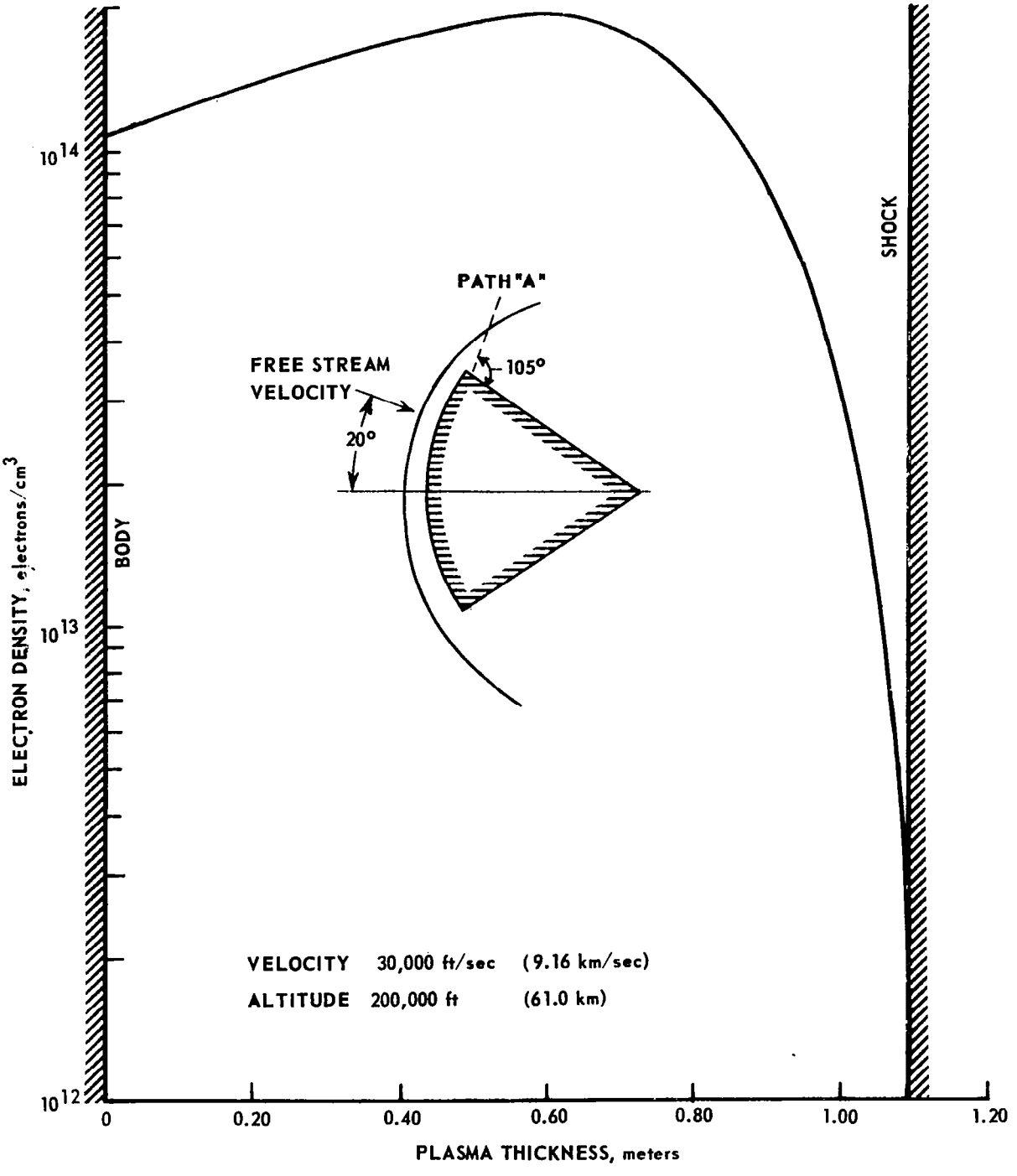

FIGURE 16 ELECTRON DENSITY DISTRIBUTION IN PLANE OF SYMMETRY FOR PATH "A"

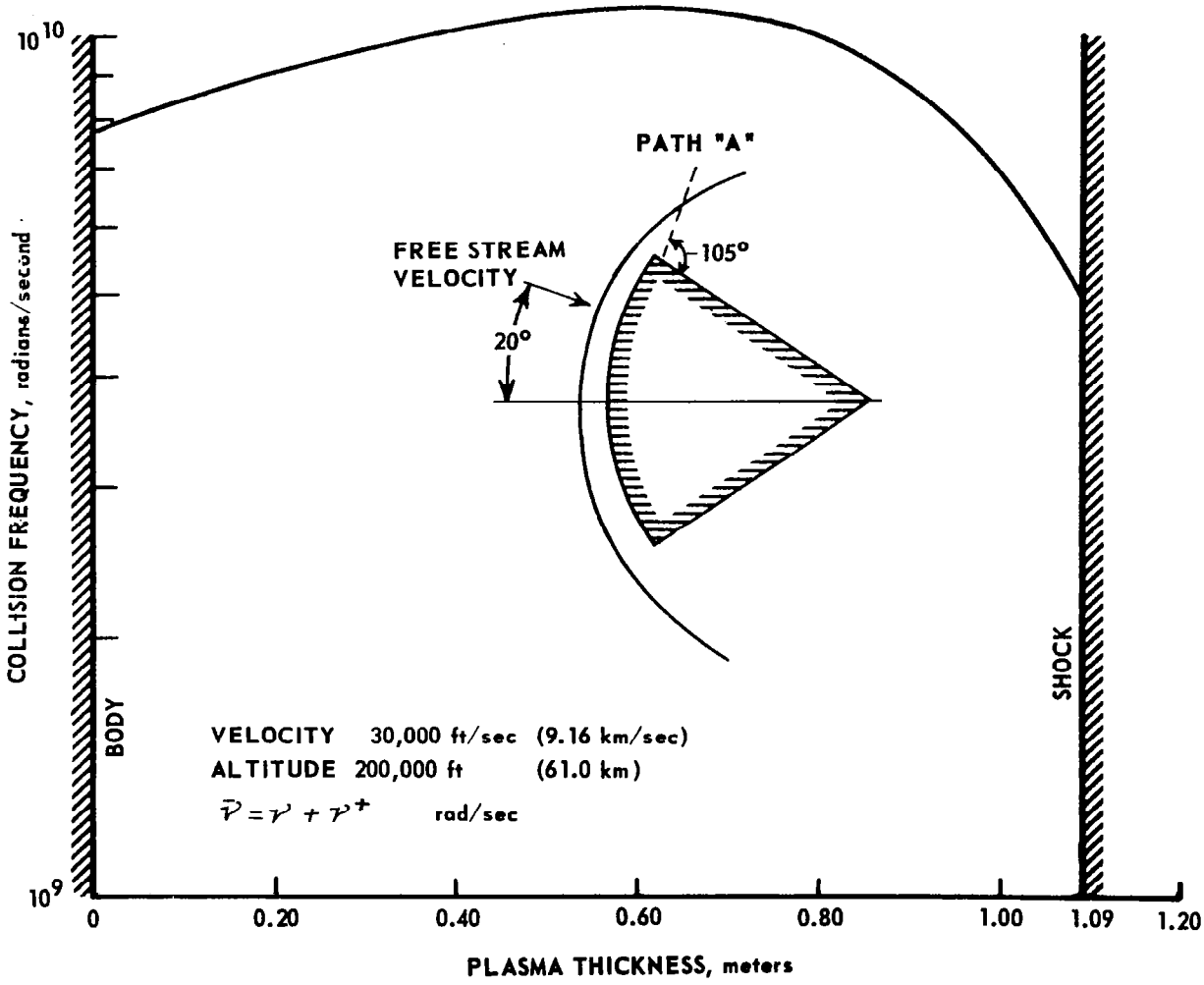

FIGURE 17 COLLISION FREQUENCY ($\bar{\nu}$) IN PLANE OF SYMMETRY FOR PATH "A"

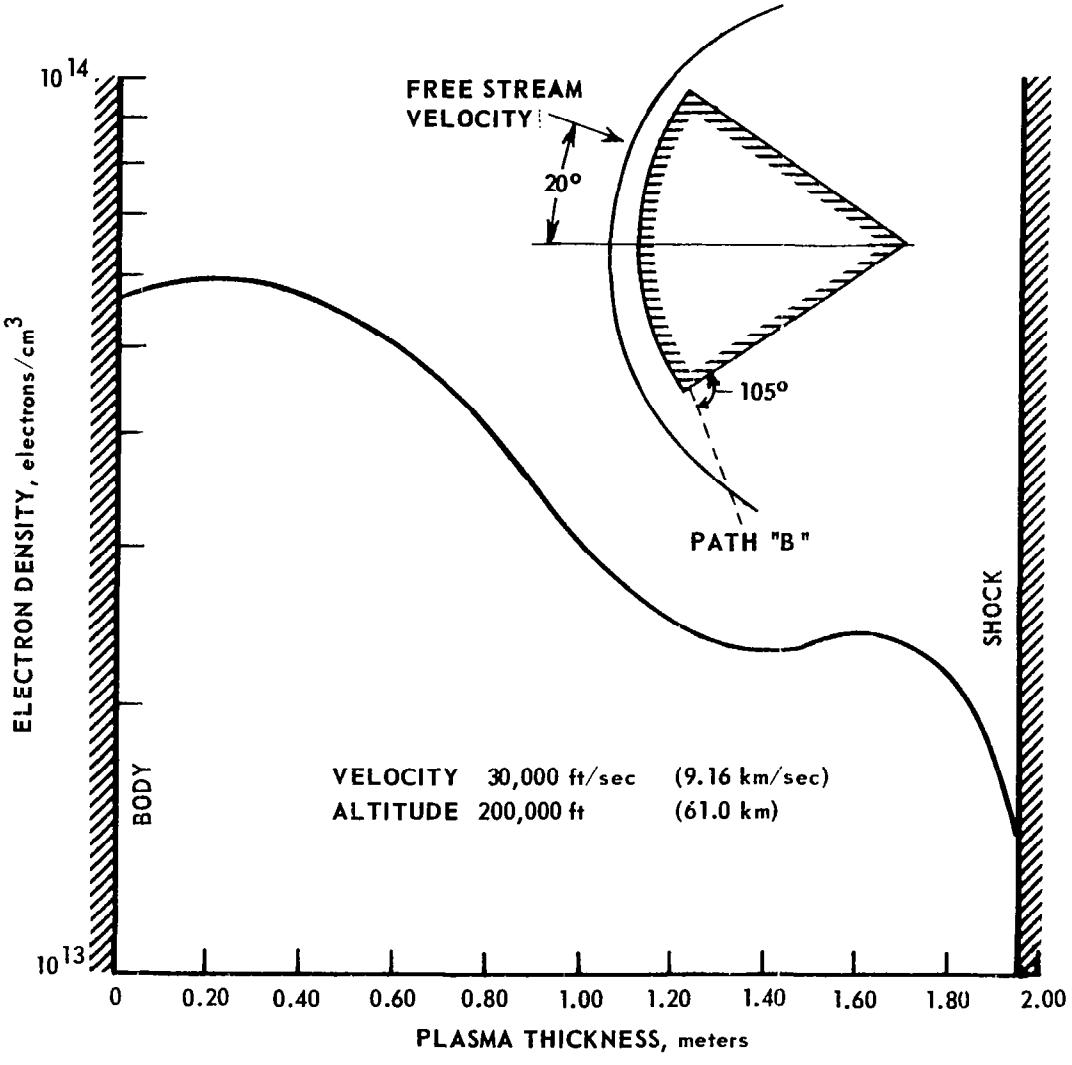

FIGURE 18 ELECTRON DENSITY DISTRIBUTION IN PLANE OF SYMMETRY PATH "B"

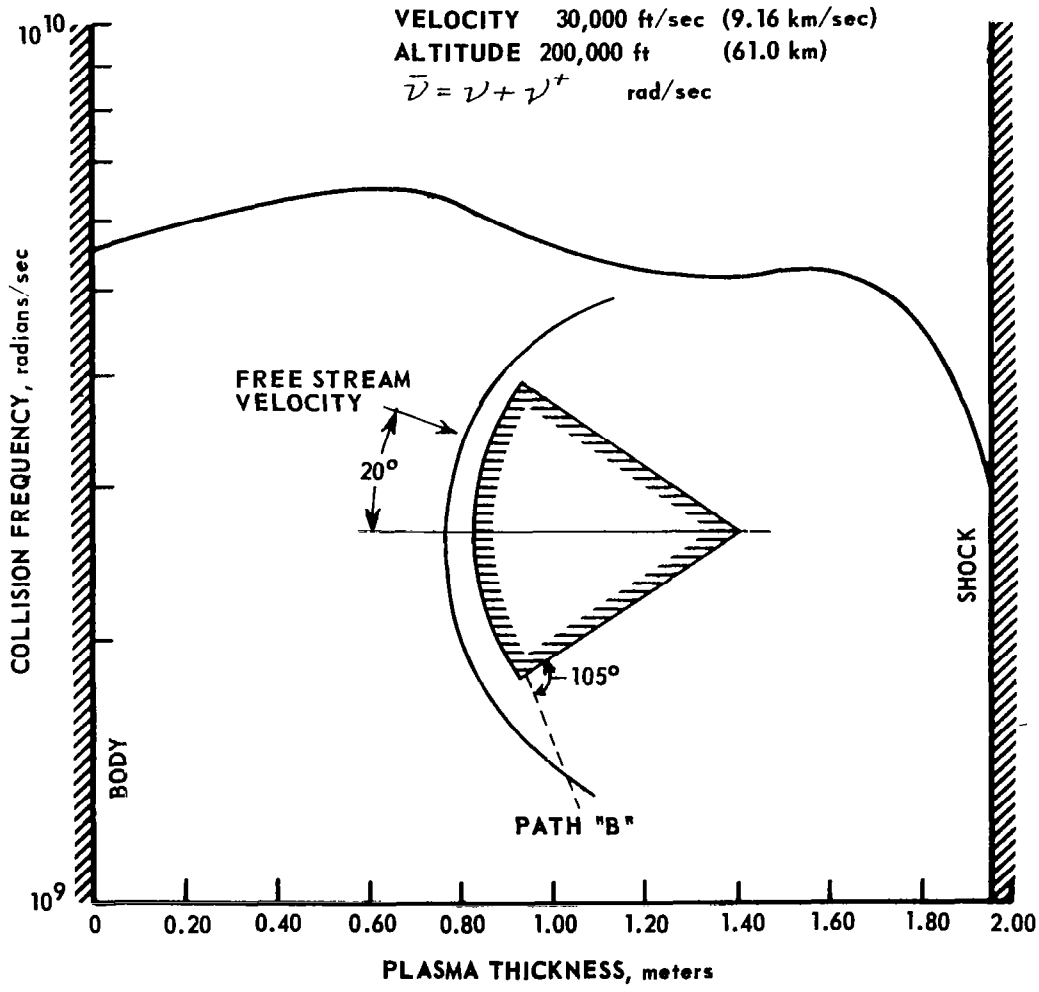

FIGURE 19 COLLISION FREQUENCY ($\bar{\nu}$) DISTRIBUTION IN PLANE OF SYMMETRY FOR PATH "B"

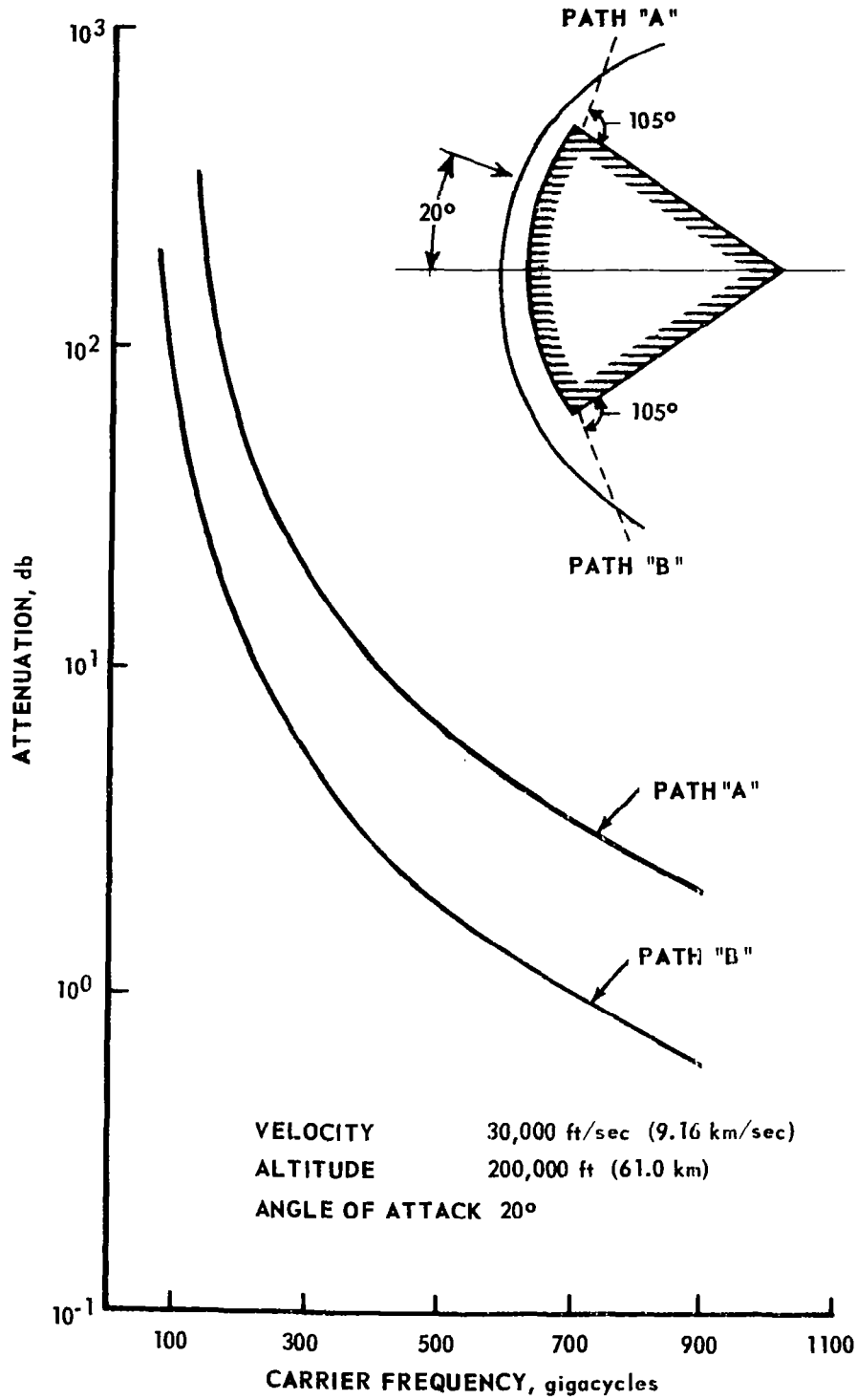

FIGURE 20 CALCULATED ATTENUATION OF ONE-DIMENSIONAL PLANE WAVES

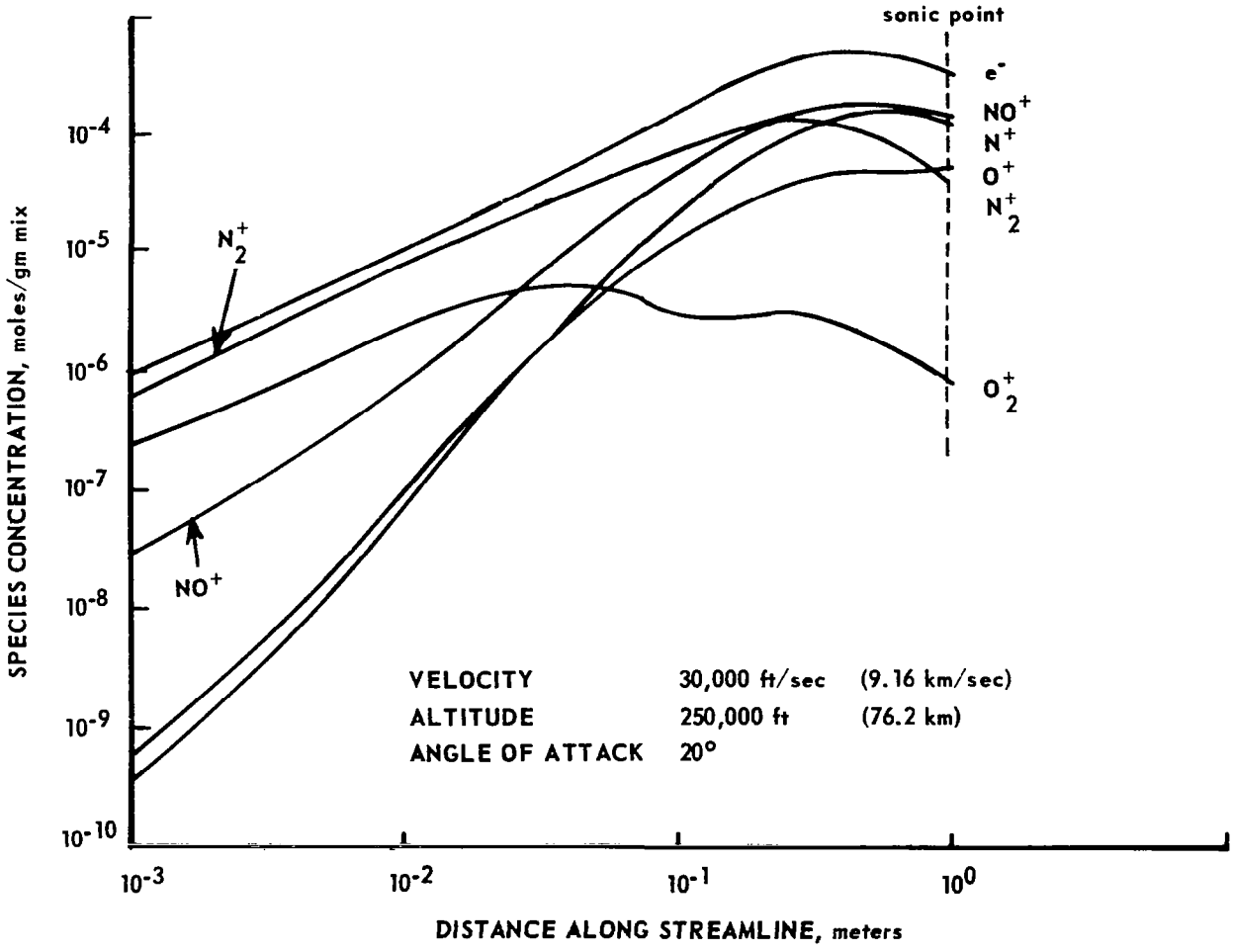

FIGURE 21 NONEQUILIBRIUM SPECIES DISTRIBUTION ALONG STREAMLINE 5 IN PLANE OF SYMMETRY

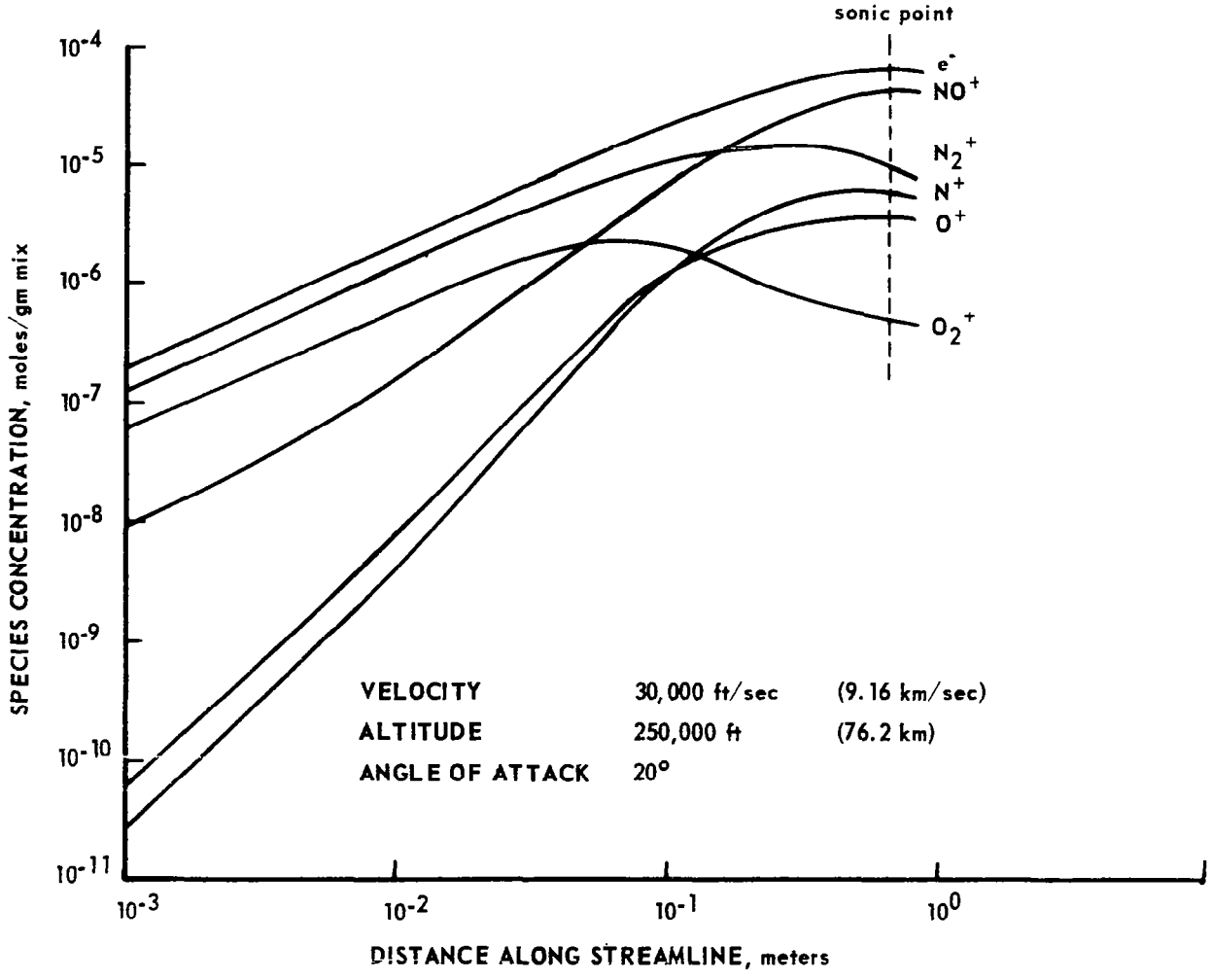

FIGURE 22 NONEQUILIBRIUM SPECIES DISTRIBUTION ALONG STREAMLINE 3 IN PLANE OF SYMMETRY

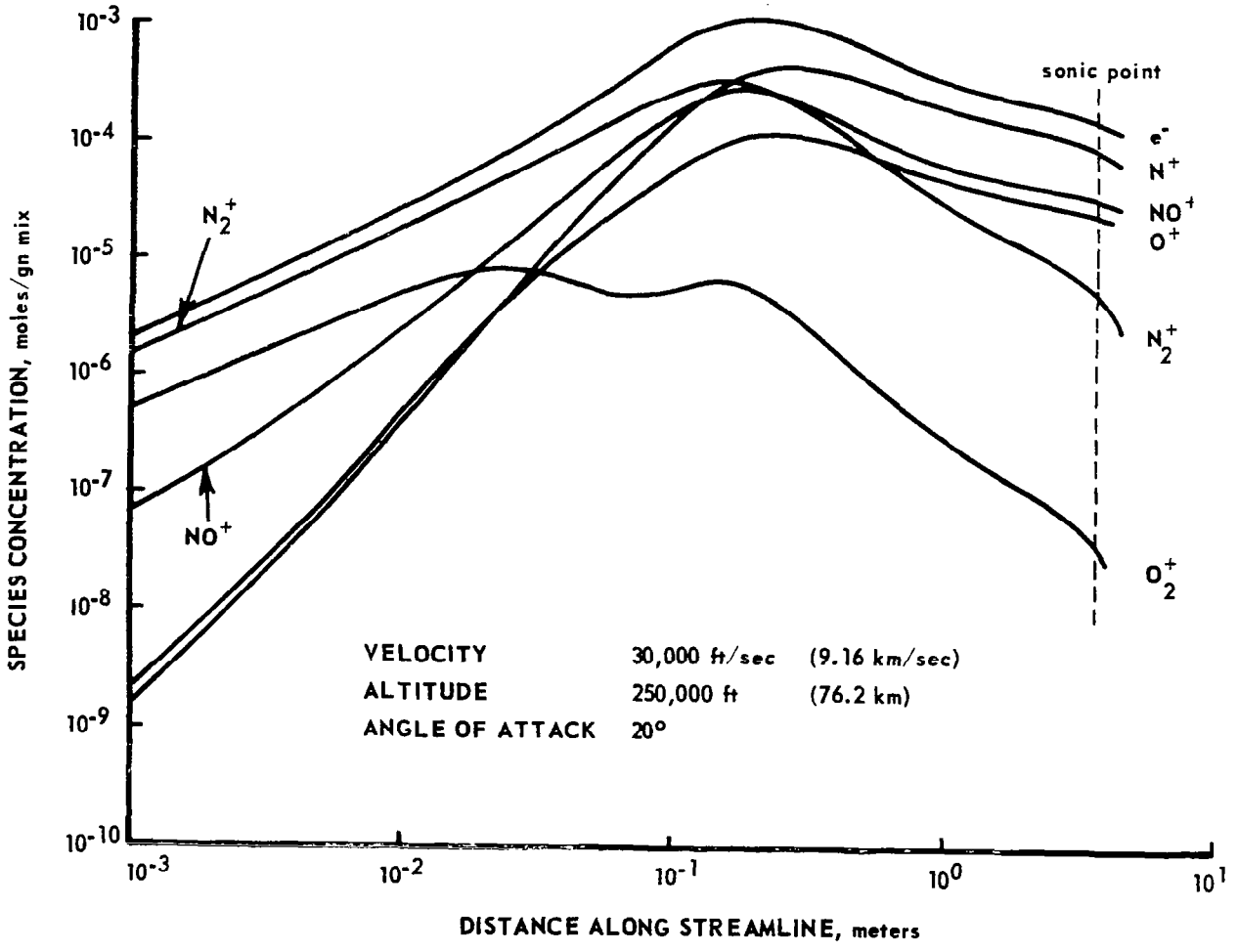

FIGURE 23 NONEQUILIBRIUM SPECIES DISTRIBUTION ALONG STREAMLINE 8 IN PLANE OF SYMMETRY

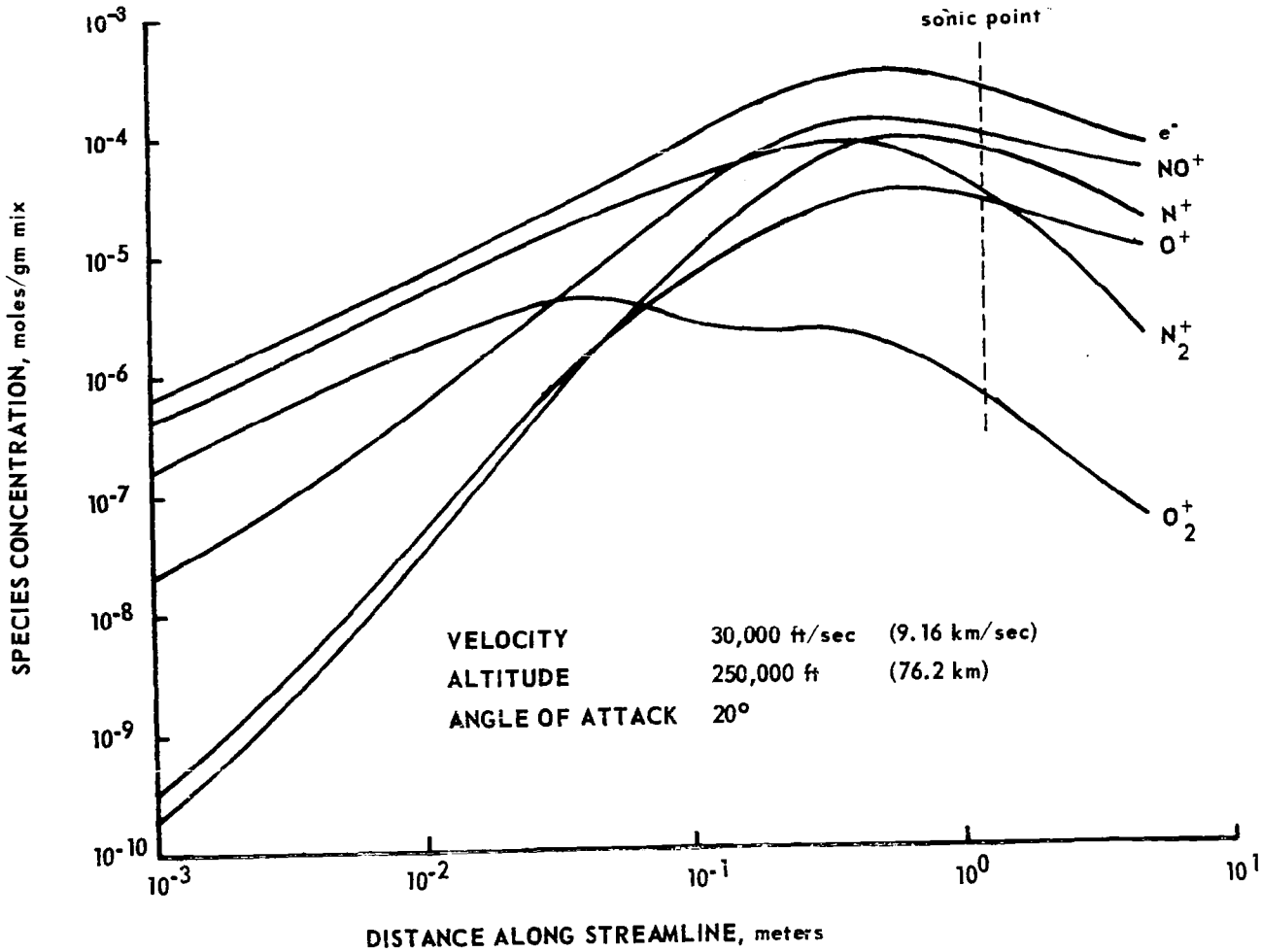

FIGURE 24 NONEQUILIBRIUM SPECIES DISTRIBUTION ALONG STREAMLINE 12 IN PLANE OF SYMMETRY

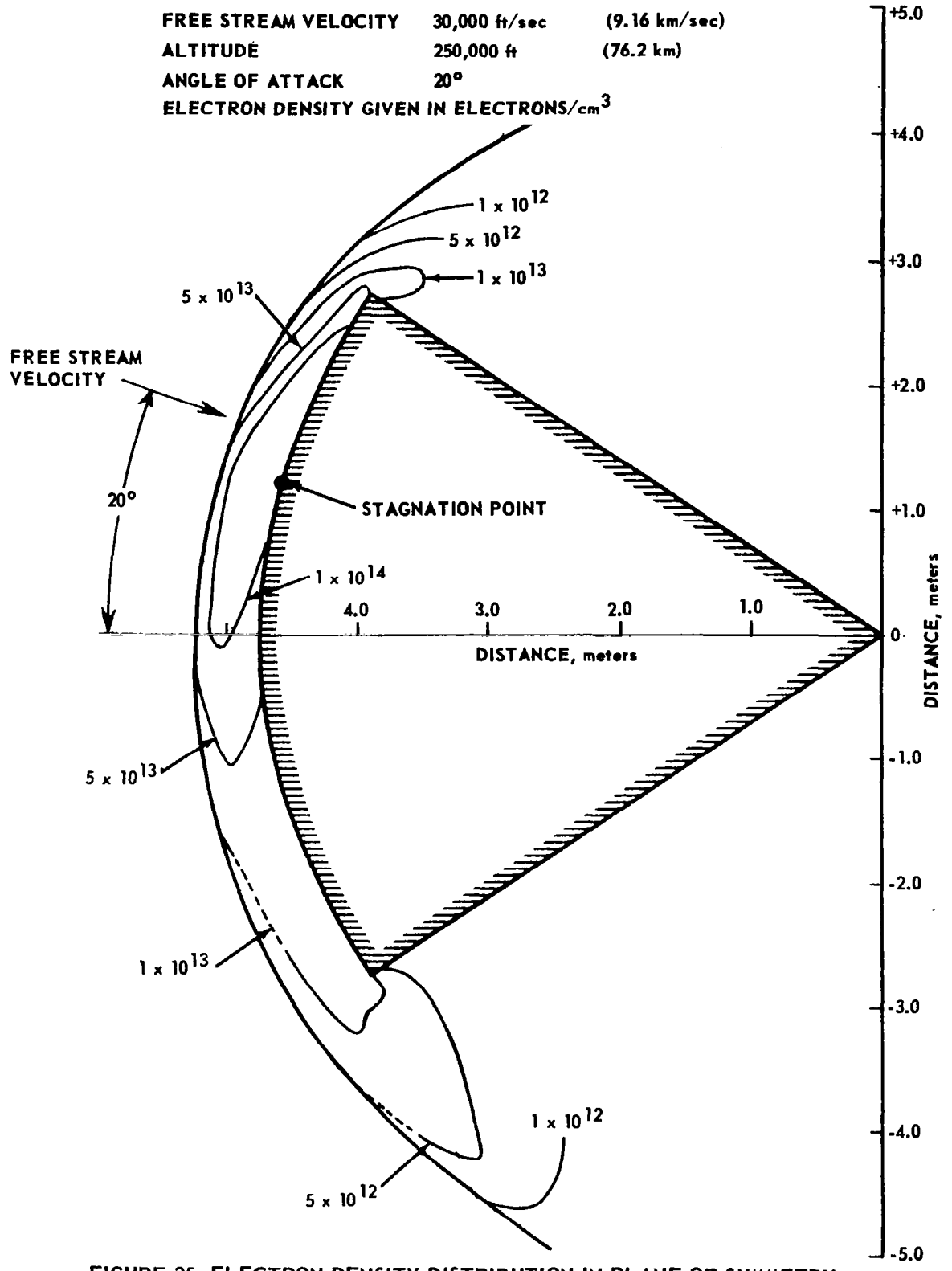

FIGURE 25 ELECTRON DENSITY DISTRIBUTION IN PLANE OF SYMMETRY

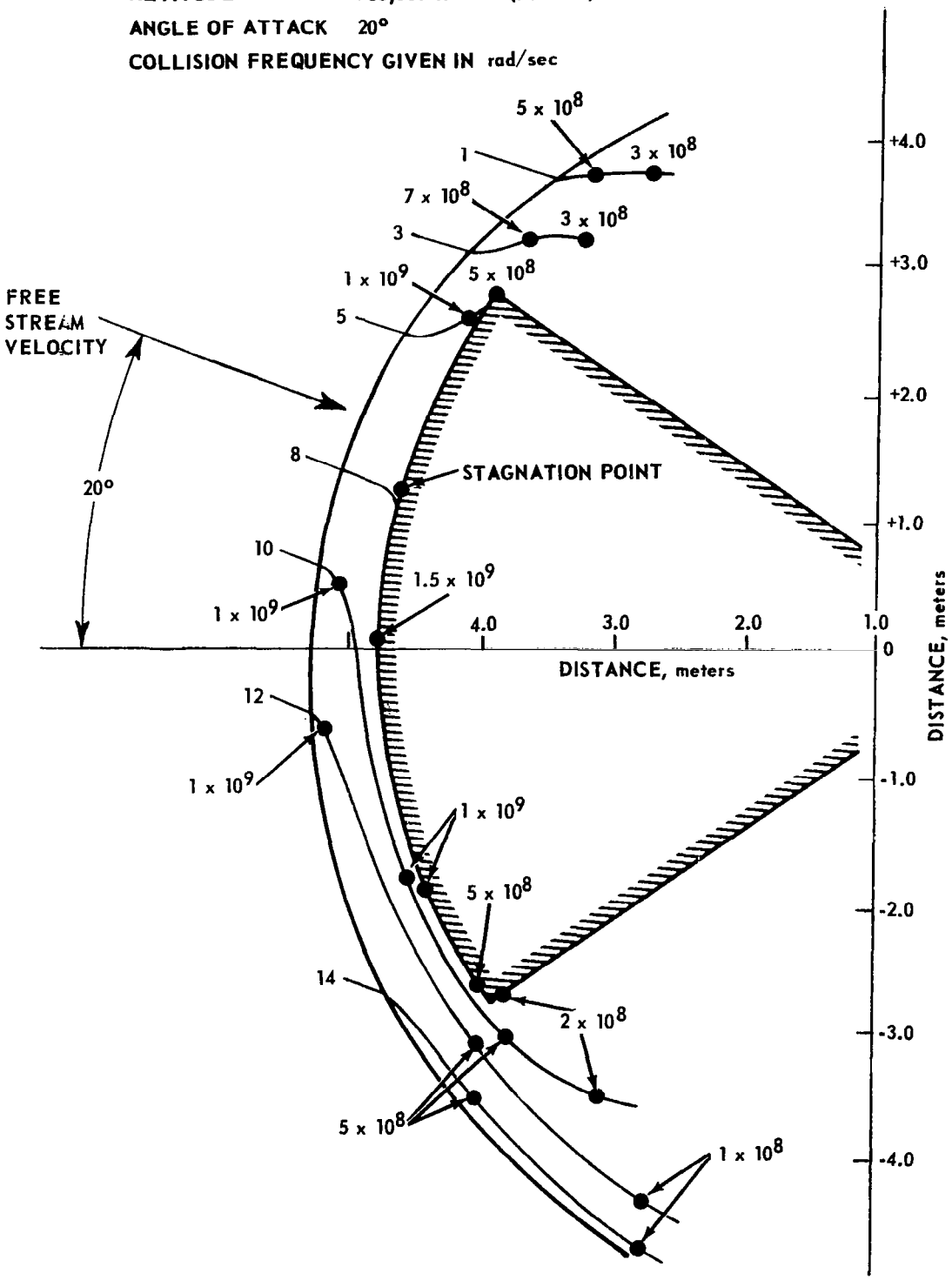

FIGURE 26 ELECTRON-NEUTRAL COLLISION FREQUENCY (ν) IN PLANE OF SYMMETRY

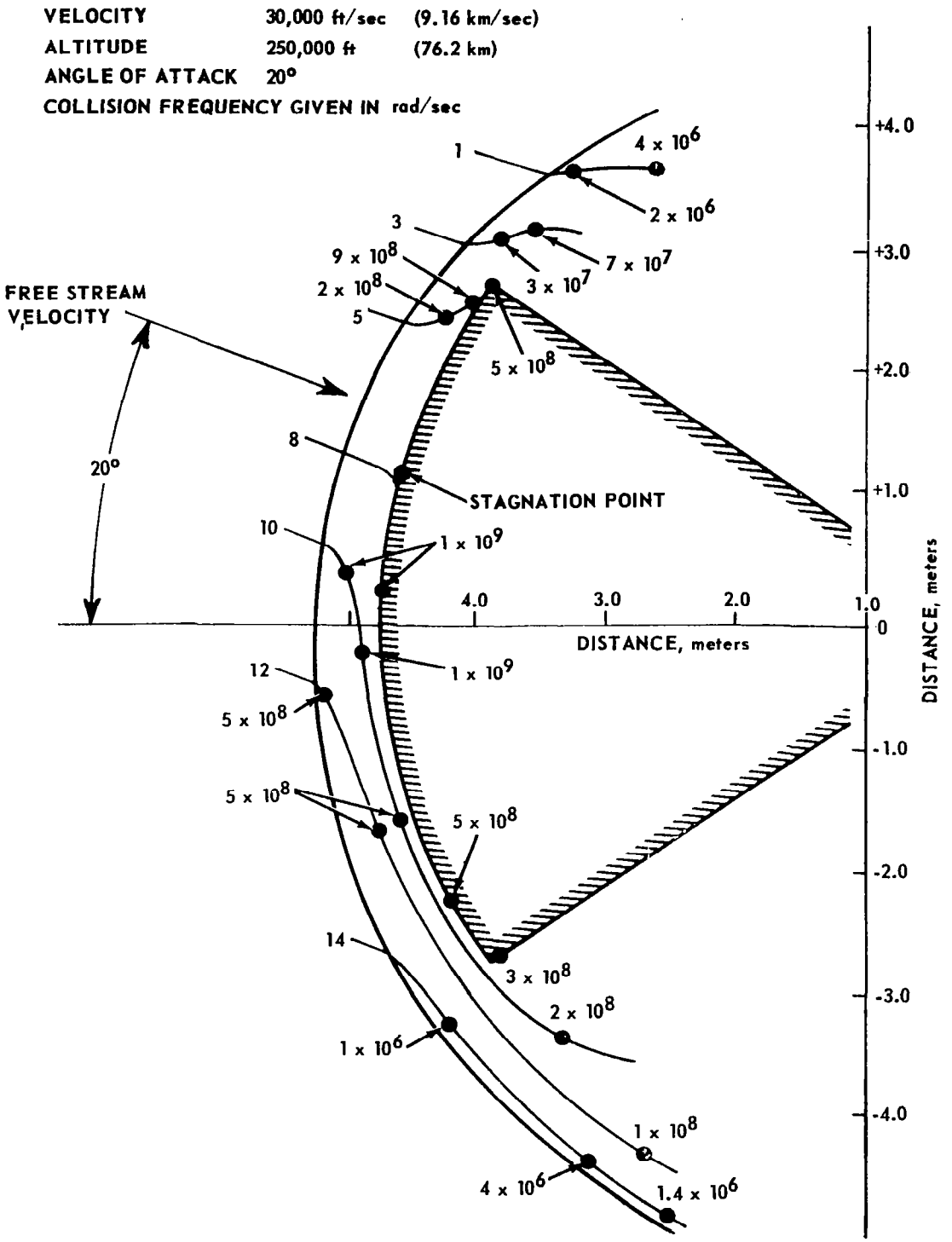

FIGURE 27 ELECTRON-ION COLLISION FREQUENCY (ν^+) IN PLANE OF SYMMETRY

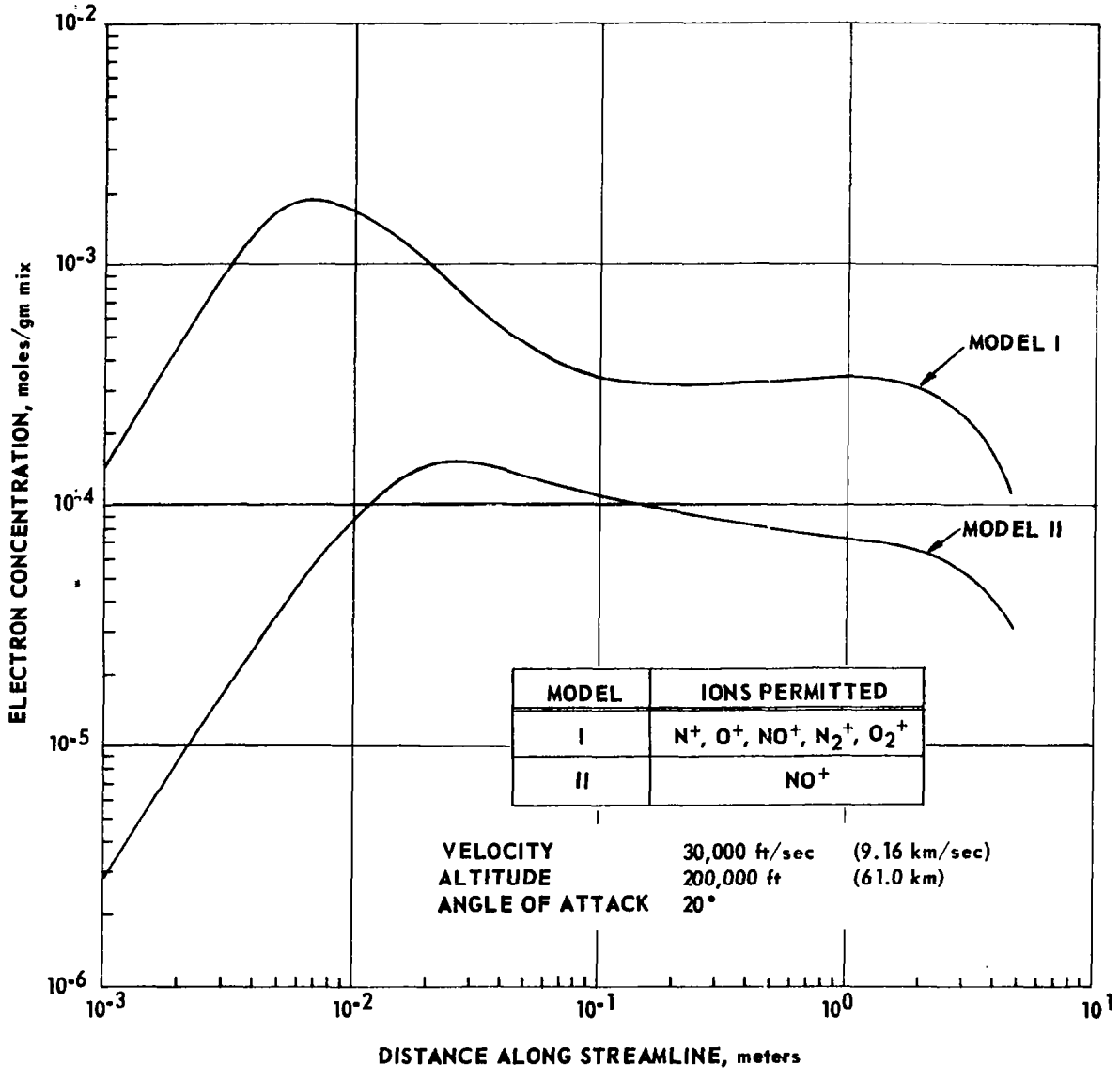

FIGURE 28 INFLUENCE OF CHARGED SPECIES TRUNCATION ON STREAMLINE 5 ELECTRON CONCENTRATION

NASA-Langley, 1966